



HAL
open science

Metal phases in ordinary chondrites: Magnetic hysteresis properties and implications for thermal history

J. Gattacceca, C. Suavet, P. Rochette, B. Weiss, M. Winklhofer, Minoru Uehara, Jon Friedrich

► To cite this version:

J. Gattacceca, C. Suavet, P. Rochette, B. Weiss, M. Winklhofer, et al.. Metal phases in ordinary chondrites: Magnetic hysteresis properties and implications for thermal history. *Meteoritics and Planetary Science*, 2014, 49 (4), pp.652-676. 10.1111/maps.12268 . hal-03289394

HAL Id: hal-03289394

<https://hal.science/hal-03289394>

Submitted on 18 Jul 2021

HAL is a multi-disciplinary open access archive for the deposit and dissemination of scientific research documents, whether they are published or not. The documents may come from teaching and research institutions in France or abroad, or from public or private research centers.

L'archive ouverte pluridisciplinaire **HAL**, est destinée au dépôt et à la diffusion de documents scientifiques de niveau recherche, publiés ou non, émanant des établissements d'enseignement et de recherche français ou étrangers, des laboratoires publics ou privés.



Distributed under a Creative Commons Attribution 4.0 International License

Metal phases in ordinary chondrites: Magnetic hysteresis properties and implications for thermal history

J. GATTACCECA^{1,2*}, C. SUAVET¹, P. ROCHETTE², B. P. WEISS¹, M. WINKLHOFFER³,
M. UEHARA², and Jon M. FRIEDRICH^{4,5}

¹Department of Earth, Atmospheric, and Planetary Sciences, Massachusetts Institute of Technology,
77 Massachusetts Avenue, Cambridge, Massachusetts 02139, USA

²CNRS, Aix-Marseille Université, CEREGE UM34, 13545 Aix en Provence, France

³Department of Earth and Environmental Sciences, Ludwig-Maximilians-University Munich,
Theresienstr. 41, D-80333 Munich, Germany

⁴Department of Chemistry, Fordham University, 441 East Fordham Road, Bronx, New York 10458, USA

⁵Department of Earth and Planetary Sciences, American Museum of Natural History, 79th Street at Central Park West,
New York City, New York 10024, USA

*Corresponding author. E-mail: gattacceca@cerege.fr

(Received 21 June 2013; revision accepted 19 December 2013)

Abstract—Magnetic properties are sensitive proxies to characterize FeNi metal phases in meteorites. We present a data set of magnetic hysteresis properties of 91 ordinary chondrite falls. We show that hysteresis properties are distinctive of individual meteorites while homogeneous among meteorite subsamples. Except for the most primitive chondrites, these properties can be explained by a mixture of multidomain kamacite that dominates the induced magnetism and tetrataenite (both in the cloudy zone as single-domain grains, and as larger multidomain grains in plessite and in the rim of zoned taenite) dominates the remanent magnetism, in agreement with previous microscopic magnetic observations. The bulk metal contents derived from magnetic measurements are in agreement with those estimated previously from chemical analyses. We evidence a decreasing metal content with increasing petrologic type in ordinary chondrites, compatible with oxidation of metal during thermal metamorphism. Types 5 and 6 ordinary chondrites have higher tetrataenite content than type 4 chondrites. This is compatible with lower cooling rates in the 650–450 °C interval for higher petrographic types (consistent with an onion-shell model), but is more likely the result of the oxidation of ordinary chondrites with increasing metamorphism. In equilibrated chondrites, shock-related transient heating events above approximately 500 °C result in the disordering of tetrataenite and associated drastic change in magnetic properties. As a good indicator of the amount of tetrataenite, hysteresis properties are a very sensitive proxy of the thermal history of ordinary chondrites, revealing low cooling rates during thermal metamorphism and high cooling rates (e.g., following shock reheating or excavation after thermal metamorphism). Our data strengthen the view that the poor magnetic recording properties of multidomain kamacite and the secondary origin of tetrataenite make equilibrated ordinary chondrites challenging targets for paleomagnetic study.

INTRODUCTION

Knowledge of the magnetic mineralogy and magnetic properties of extraterrestrial materials is crucial for interpreting the paleomagnetism of meteorites (see Weiss et al. [2010] for a review), for

interpreting the magnetic anomalies of planetary surfaces (e.g., Dunlop and Kletetschka 2001; Wasilewski et al. 2002; Arkani-Hamed 2005; Rochette et al. 2005 for Mars; Rochette et al. 2010; Wieczorek et al. 2012 for the Moon). It also sheds light on the redox conditions prevailing during the formation of solid

matter in the solar system (e.g., Rochette et al. 2008), and on its evolution through time. Intrinsic magnetic properties, in particular susceptibility, can be used as a rapid classification tool (Rochette et al. 2003, 2008, 2009), allowing scanning of large meteorite collections for preliminary classification (Folco et al. 2006) or in search of anomalous samples (e.g., Kohout et al. 2010), and with potential application to the characterization of asteroids (Kohout et al. 2008). The anisotropy of magnetic susceptibility has been used to study the compaction history of chondrites (Sneyd et al. 1988; Gattacceca et al. 2005).

Most comprehensive studies about the magnetic properties of meteorites were focused on magnetic susceptibility (e.g., Rochette et al. 2003, 2008, 2009), magnetic anisotropy (Gattacceca et al. 2005, 2008), and thermomagnetic behavior (e.g., Lovering and Parry 1962; Herndon et al. 1976; Nagata and Funaki 1982; Momose and Nagai 1983). In contrast, little is known about the magnetic hysteresis properties of meteorites, particularly for metal-bearing stony meteorites. Hysteresis properties are sensitive proxies of grain size (e.g., Peters and Dekkers 2003), the presence of defects in the crystal structure (e.g., Ozdemir and Dunlop 1997), and the bulk abundances of magnetic minerals. In particular, hysteresis properties are very sensitive to the microstructures of metal grains and may thus be a good proxy of the thermal history of meteorites (e.g., Leroux et al. 2000).

Hysteresis properties of 22 meteorites, including 14 ordinary chondrites, were measured by Sugiura (1977), but most of these are Antarctic finds whose magnetic properties are likely to be affected by terrestrial weathering (Uehara et al. 2012). The only significant data set of hysteresis properties for meteorite falls is the report by Terho et al. (1992) that provides hysteresis parameters for 26 ordinary chondrite falls. However, no detailed interpretation is given in this report and a subsequent publication (Pesonen et al. 1993).

In this study, we present magnetic hysteresis properties of 91 ordinary chondrite falls. Data for 10 HEDs (howardites, eucrites, diogenites) achondrites are also provided for comparison. This data set, based mainly on new measurements, is the basis for a discussion on the magnetic mineralogy of ordinary chondrites, its relation with the thermal and shock history of meteorites, and the implications for paleomagnetism.

SAMPLES AND METHODS

Samples

Only meteorite falls were studied to avoid biases due to terrestrial weathering and the associated

formation of ferric phases (in particular, maghemite) in meteorites finds (Kohout et al. 2004; Bland et al. 2006). Weathering has been shown to drastically modify the hysteresis properties of ordinary chondrites even at its incipient stages (Uehara et al. 2012). In this study, we increase the hysteresis properties database significantly with new measurements on 109 ordinary chondrite samples representing 70 different meteorites. Sample selection was made to span the three ordinary chondrite classes (H, L, and LL), as well as a few chondrites from the intermediate classes H/L and L/LL (Kallemeyn et al. 1989). In each class, we selected samples spanning the whole spectrum of thermal metamorphism, from type 3 to type 6 (as defined by Van Schmus and Wood 1967). For the L class, we also selected samples spanning all six levels of shock, from stages S1 to S6 (as defined by Stöffler et al. 1991). For all three classes, meteorites of metamorphic type 3 are overrepresented in our database with respect to the average population, but types 4 to 6 are represented approximately correctly relative to one another. For L chondrites, heavily shocked meteorites of shock stage S4 and above are also overrepresented. For comparison with meteorites containing FeNi minerals but with completely different petrogenetic and thermal histories, 19 HED samples were also studied. Studied samples range from 20 mg to 3 g in mass. Most samples are from the collection of the Muséum National d'Histoire Naturelle (MNHN, Paris, France).

Magnetic Measurements

Readers not familiar with the measurement and meaning of rock magnetic parameters may refer to Collinson (1983) and Dunlop and Özdemir (1997) for in-depth explanations. Magnetic hysteresis properties were measured with a Princeton Micromag vibrating sample magnetometer (VSM) with a noise level of about 1 nAm^2 and a maximum applied field of 1 T. Hysteresis loops allow the determination of coercivity (B_C), saturation magnetization (M_S), saturation remanent magnetization (M_{RS}), high-field susceptibility (χ_{HF} , including both diamagnetic and paramagnetic contributions). Coercivity of remanence (B_{CR}) was evaluated through DC back-field demagnetization of the saturation remanence. Saturation remanent magnetization was also measured with a 2G DC SQUID magnetometer model 755R (noise level 10^{-11} Am^2) after saturation in a 1 T field using a pulse magnetizer from Magnetic Measurements. The M_{RS} value measured this way is more accurate than that obtained with the VSM (whose measurements are more sensitive to the geometry of the sample) and was used to recalculate the M_S through the M_{RS}/M_S ratio

provided by the VSM. First-order reversal curves (FORC) were acquired using the same VSM using a field sampling interval of 10 mT. FORC data were processed with a smoothing factor of three using UNIFORC software (Egli et al. 2010). Mass normalized low-field magnetic susceptibility χ of the same samples was measured in an AC field of 200 A m⁻¹ (peak field) and frequency 976 Hz with a MFK1 apparatus from Agico (sensitivity 5×10^{-13} m³). Magnetic susceptibility was measured along three orthogonal directions and averaged to account for the variability introduced by the often strong magnetic anisotropy of FeNi-bearing meteorites (Gattacceca et al. 2005). The ferromagnetic susceptibility was then computed as $\chi_f = \chi - \chi_{HF}$. All magnetic measurements were performed at CEREGE (Aix-en-Provence, France). Previous hysteresis data (Nagata and Sugiura 1976; Sugiura 1977; Nagata et al. 1986; Terho et al. 1992) were included in our database only for meteorites that were not measured in our study, amounting to 21 meteorites.

Because grain shape can affect some magnetic properties (like apparent magnetic susceptibility), X-ray microtomography was used to evaluate the shape of metal grains in some ordinary chondrites. Data were collected at resolutions of 13–19 $\mu\text{m}/\text{voxel}$ with monochromatic X-rays using the 13-BMD beamline located at the Advanced Photon Source (APS) of Argonne National Laboratory. These resolutions are known to be adequate for observing the morphology and size distributions of metal and sulfide grains in ordinary and other chondrites (Friedrich et al. 2008). Details of the data collection can be found in Friedrich et al. (2008, 2013). Three-dimensional examination of ordinary chondrite metal grain shapes was accomplished digitally isolating them in images and computing best fitting ellipsoids following Friedrich et al. (2008). Metal grain shapes were inferred from major, intermediate, and short ellipsoid axes using the Zingg (1935) parameters and nomenclature.

Anisotropy Effects

Anisotropy of magnetic susceptibility in ordinary chondrites is strong, ubiquitous, and controlled mostly by the preferential alignment of metallic grains (Gattacceca et al. 2005). Remanence anisotropy can also be strong in ordinary chondrites because of the crystalline anisotropy of tetrataenite (e.g., Gattacceca et al. 2003). Therefore, measurement of hysteresis properties along a single direction may result in a significant departure from the anisotropy-averaged value.

Measurements on eight 0.4 g cubic samples of the Bensour LL6 chondrite reveal an average anisotropy

degree (ratio of maximum to minimum value) of 1.28 ± 0.08 for M_{RS} . In such a meteorite, measurement of M_{RS} along a single direction may result in a maximum departure of $\pm 12\%$ from the anisotropy-averaged value. Measurements on 0.5 g cubic samples of Pultusk H4 chondrite give an anisotropy degree of 1.18 for M_{RS} , indicating a maximum departure of $\pm 8\%$ from the average value. B_{CR} values for the same Pultusk samples differ by up to 20% from the average value. Therefore, the effects of magnetic anisotropy can significantly bias M_{RS} and B_{CR} (up to approximately 10 and approximately 20%, respectively) if hysteresis is measured along a single random axis. This is especially true for LL chondrites that have stronger remanence anisotropy than L and H chondrites because of the higher relative abundance of tetrataenite. However, measurements of several randomly oriented samples help to minimize this bias, an approach that has been used for most LL chondrites studied in this study with an average of three samples (and up to 15 samples) measured per meteorite.

Approach to Saturation

In most previous studies that provided hysteresis measurements on FeNi-bearing meteorites (or lunar rocks), saturation magnetization was computed after subtracting the contribution of paramagnetism and diamagnetism estimated by a linear fit of the reversible part of the hysteresis loop (generally in the 0.8–1 T or 0.9–1 T interval to take into account the nonsaturation of FeNi multidomain grains below approximately 0.7 T). However, in the reversible part of a hysteresis loop, the magnetization M does not increase strictly linearly with applied field B , but is better expressed as $M = M_S + \chi_{HF} B + \alpha B^\beta$ (e.g., Fabian 2006). α and β are negative parameters that are mineral dependent. In most cases, the term αB^β is negligible, and χ_{HF} and M_S are well approximated by a linear fit of the reversible part of the hysteresis loops. However, as shown below, this approximation does not hold for ordinary chondrites and leads to underestimation of M_S and overestimation of χ_{HF} . Instead, we used the approach to saturation method to estimate M_S and χ_{HF} . α was determined for each meteorite, so as to minimize the residual of the linear regression of $M - \alpha B^\beta$ where we assumed $\beta = -2$, the theoretical and observed value for defect free minerals (Fabian 2006). M_S and χ_{HF} are the intercept and slope of the regression, respectively. The regressions were computed on the $|B| > 0.8$ T portions for all four branches of the hysteresis cycle. This algorithm was tested on a hysteresis loop measured at room temperature on a sample made of 76 wt% of gadolinium oxide (70 mg of Gd₂O₃ from Aldrich with a theoretical paramagnetic

susceptibility of $1.85 \times 10^{-6} \text{ m}^3 \text{ kg}^{-1}$; see Sagnotti et al. 2003) and 24 wt% metallic iron (10 μm synthetic powder in multidomain state from Merck), with a theoretical $M_S = 218 \text{ Am}^2 \text{ kg}^{-1}$, a proportion roughly similar to that found in H ordinary chondrites. The algorithm gave a reliable value for M_S with a departure from the theoretical value of only 0.6%, whereas the classic linear fit underestimates the theoretical value by 17%. χ_{HF} is overestimated by a factor of 2.2 when using the linear fit, and is underestimated by a factor of 3.7 when using the approach to saturation. In conclusion, the approach to saturation provides a more reliable estimate for M_S (and thus the mass content of metallic iron), but fails to provide a reliable estimate of χ_{HF} because the magnetization of metallic iron is too strong and masks the signal from paramagnetic minerals.

Most hysteresis loops measured in this study were processed using approach to saturation. We find that a linear fit in the 0.9–1 T interval on average underestimates M_S by 19% (SD 7%, $n = 68$). For the few loops that were noisy at high fields (above approximately 0.7 T) and could not be processed using approach to saturation, we used a linear fit in the 0.9–1 T and corrected the M_S value using this 19% underestimate. It is noteworthy that approach to saturation is applicable only on the reversible part of the hysteresis loops, and is not strictly applicable to samples that are not saturated in a field of 1 T, the maximum field used for our measurements. A few tetrataenite-dominated chondrites (as identified by their higher B_{CR} , see Hysteresis Properties in Different Ordinary Chondrite Classes section) are clearly not saturated in 1 T (e.g., Guidder in Fig. 1A), leading to underestimation of M_S when using both a linear fit in the 0.9–1 T range or the approach to saturation.

INTRODUCTION TO FERROMAGNETIC MINERALS IN ORDINARY CHONDRITES

Before presenting the results of our hysteresis measurements, we give a brief overview of the magnetic minerals that are found in ordinary chondrites and their magnetic properties. With the exception of magnetite and cohenite that are present in some of the most unequilibrated chondrites like Semarkona (Hutchison et al. 1987; Krot et al. 1997), the only significant ferromagnetic minerals at room temperature are metallic FeNi alloys. These alloys are found mostly in the form of kamacite (α bcc, with ~ 5 wt% Ni), taenite (γ fcc, with 10–50 wt% Ni, but paramagnetic at room temperature for Ni < 30 wt%), tetrataenite (γ'' ordered tetragonal, approximately 50 wt% Ni), martensite (metastable distorted bcc), and rare awaruite (γ' ordered FeNi_3). These minerals can exist as a single phase, like

kamacite that forms homogeneous grains up to several 100 μm , or can form complex microstructures such as plessite and zoned taenite (e.g., Reisener and Goldstein 2003; Yang et al. 1997a; Uehara et al. 2011). Plessite is a fine-grained ($< 10 \mu\text{m}$) intergrowth of kamacite and tetrataenite formed during decomposition of martensite below 500–300 °C (depending on the local Ni content) and down to temperatures below 200 °C (Reisener and Goldstein 2003; Goldstein and Michael 2006). Plessite can also be formed by reheating martensite in the kamacite + taenite stability field, i.e., between 400 °C and 700 °C depending on the local Ni content.

We note that the terminology used in metallography and cosmochemistry studies is not always sufficient for a detailed understanding of magnetic properties. For instance, “taenite” grains are usually compositionally zoned in equilibrated ordinary chondrites, and they actually contain not only taenite (in relatively small amounts) but also a tetrataenite rim, a cloudy zone, and a martensite and/or plessite core (Scott 1973; Reisener and Goldstein 2003). The cloudy zone is composed of tetrataenite islands in a kamacite/martensite matrix, although the nature of the matrix is still debated (Bryson et al. 2014). As a result, even though the average Ni content of such “taenite” is about 35 wt% Ni in ordinary chondrites (Afiattalab and Wasson 1980; Smith et al. 1993), this value likely represents an average value of fine tetrataenite grains with approximately 50 wt% Ni and paramagnetic taenite with less than 30 wt% Ni, as already discussed by, e.g., Nagata et al. (1986). Another example of this is the Santa Catharina Ni-rich ataxite, in which regions composed of pure cloudy zone described as tetrataenite islands of approximately 20 nm in a taenite matrix also have a bulk composition of 35 wt% Ni (Danon et al. 1979a; Zhang et al. 1990). Another issue is that tetrataenite is often reported in chondrites based on microprobe analyses only. But chemical analyses alone cannot distinguish between tetrataenite (formed by slow cooling) and taenite (formed by fast cooling) with the same composition. For instance, an approximately 100 μm euhedral “tetrataenite” grain described in an impact melt rock clast in the Jelica LL6 chondrite (Rubin 1994) is likely to be taenite in view of its position in a quenched impact melt rock. Similarly, the “tetrataenite” grains described in Semarkona (LL3.00) and Krymka (LL3.2) based on elemental analyses only (Rambaldi and Wasson 1984; Reisener and Goldstein 1999) are unlikely to be ordered in view of the low metamorphism temperature suffered by these meteorites, but are more likely nickel-rich taenite.

Examination of the FeNi phase diagram (e.g., Reuter et al. 1989; Yang et al. 1997a) shows that any taenite in slowly cooled meteorites should have a Ni

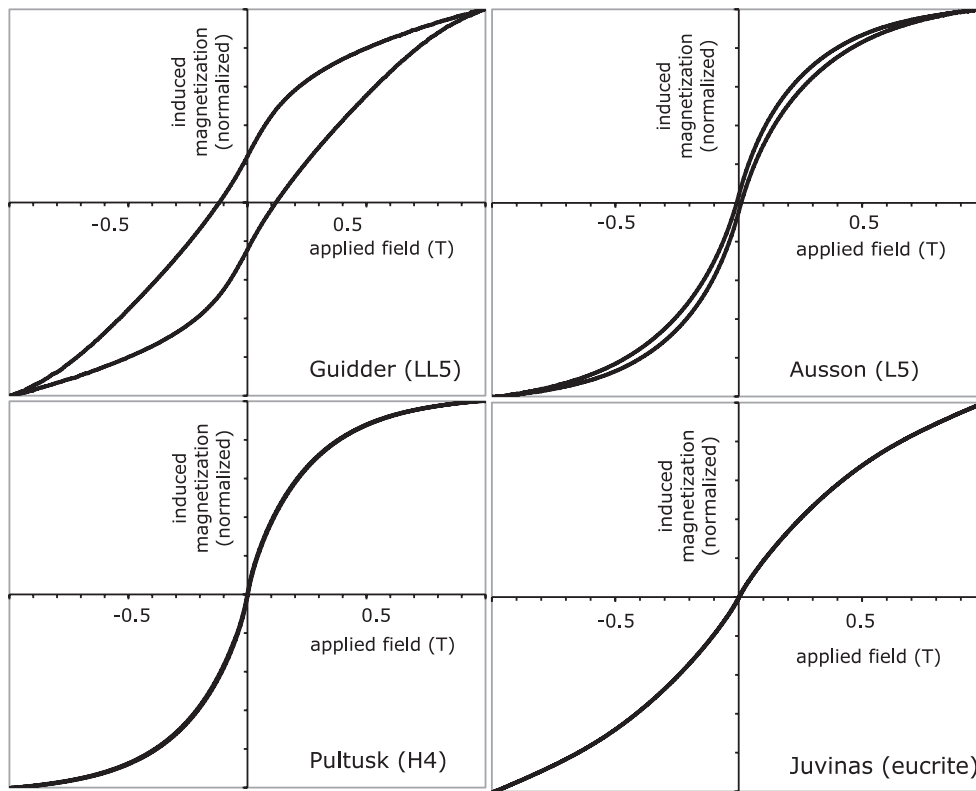


Fig. 1. Representative hysteresis loops: Gudder (LL5), Ausson (L5), Pultusk (H4), Juvinas (eucrite). The data are displayed before correction for high-field susceptibility.

content below 30 wt% Ni (γ_1 phase), otherwise it would have decomposed by entering the spinodal region on cooling below 400–300 °C. As a consequence, any taenite in slowly cooled meteorites should be paramagnetic at room temperature (Crangle and Hallam 1963). This is confirmed by Mössbauer spectroscopy of the metallic phases of some ordinary chondrites (e.g., Nagata et al. 1986). However, the presence of room temperature ferromagnetic taenite (i.e., with Ni > 30 wt%) has also been detected by Mössbauer spectroscopy in two other ordinary chondrites (Scorzelli et al. 1994; Kong and Ebihara 1996), sometimes in very significant amounts, suggesting nonequilibrium processes like fast postshock cooling or unusual cooling histories with initial slow cooling down to approximately 400°C, allowing formation of Ni-rich taenite followed by quenching that prevented decomposition into tetrataenite. Indeed, because of the slow solid state diffusion of Ni in FeNi (see, e.g., Hopfe and Goldstein 2001), thermodynamic equilibrium is not easily reached at low temperatures.

The formation of tetrataenite also requires a low cooling rate. Tetrataenite has been found in iron meteorites with metallographically determined cooling rates in the 650–400 °C range of up to several

thousands of °C Myr⁻¹, but is absent in shock reheated iron meteorites (Scott 1973; Goldstein et al. 2009). Petrographic observations also show the absence of taenite with Ni concentrations inside the tetrataenite range in slowly cooled equilibrated ordinary chondrites, except in the reheated zone close to the fusion crust (Clarke and Scott 1980). However, the exact cooling rate limit that allows formation of tetrataenite is not known as experiments cannot access this low cooling rate range, and numerical simulations have not been performed for the low-temperature range of the FeNi diagram (Mishin et al. 2005).

Combination of bulk and microprobe chemical analyses indicates that kamacite makes up to 88, 76, and 0–53 wt% of FeNi metal in H, L, and LL chondrites, respectively (Afiatalab and Wasson 1980). The tetrataenite, kamacite, and paramagnetic taenite contents in equilibrated ordinary chondrites were estimated by Mössbauer spectroscopy on a limited number of ordinary chondrite falls (Danon et al. 1979b; Nagata et al. 1986, 1991). The average kamacite, tetrataenite, and paramagnetic taenite contents computed from these measurements are reported in Table 1. There is a fair agreement between the kamacite content based on chemical analyses and Mössbauer

Table 1. FeNi mineralogy in ordinary chondrites.

Technique	wt% metal	wt% Ni in metal	Fraction of kamacite in metal (wt%)		Fraction of tetrataenite in metal (wt%)		Fraction of M_{RS} carried by kamacite %
	Chemical analyses	Chemical analysis	Chemical analysis	Mössbauer	Mössbauer	Fraction of M_S carried by kamacite %	M_{RS} carried by kamacite %
References	^a	a	b	c	c	d	d
H	18.20 ± 1.44 ($N = 25$)	10 ($N = 28$)	88	65 ($N = 1$)	18 ($N = 1$)	89	48
H/L	13.79 ($N = 1$)	12 ($N = 1$)					
L	8.45 ± 0.81 ($N = 53$)	15 ($N = 54$)	76	80 ± 6 ($N = 2$)	12 ($N = 2$)	83	22
L/LL	6.57 ± 1.16 ($N = 2$)	16 ($N = 2$)					
LL	2.94 ± 1.51 ($N = 14$)	30 ($N = 14$)	53	35 ± 16 ($N = 6$)	49 ($N = 6$)	56	3

^aComputed from Jarosewich (1990).

^bAfiattalab and Wasson (1980).

^cComputed using data on meteorite falls from Danon et al. (1979b); Nagata et al. (1986, 1991) (Mössbauer spectroscopy). For L chondrites, data for Shaw meteorite are not included based on its peculiar shock history (Danon et al. 1979b). For LL chondrites, Tuxtuac is an outlier and has not been included.

^dSee text (see Contribution of Kamacite and Tetrataenite section).

Table 2. Intrinsic magnetic properties of FeNi minerals found in ordinary chondrites.

Mineral	Structure	Mean Ni wt%	$(Am^2 kg^{-1})$	$\chi (m^3 kg^{-1})$	Single-domain size	
					Lower (nm)	Upper (nm)
Kamacite	bcc	6.4 ^a	224 ^c	544 10 ^{-6h,i}	20 ^j	~20 ^j
Martensite	Distorted bcc	8–30 ^b				
Taenite ^l	fcc	25 ^a				
Tetrataenite	Ordered tetragonal	50 ^a	130 ^d , 155 ^e , 143 ^f , 160 ^g		7 ^d	80–90 ^k

^aAfiattalab and Wasson (1980).

^bSmith et al. (1993).

^cCrangle and Hallam (1963).

^dNagata et al. (1991).

^eNéel et al. (1964) on synthetic tetrataenite.

^fFunaki et al. (1986) on multidomain tetrataenite.

^gNagata et al. (1986) on single-domain tetrataenite using Santa Catharina meteorite that contains only single-domain tetrataenite as ferromagnetic mineral (Danon et al. 1979a; Zhang et al. 1990).

^hRochette et al. (2009) on multidomain iron spheres.

ⁱNagata et al. (1975) on a EH3 chondrite with only multidomain kamacite as ferromagnetic mineral.

^jButler and Banerjee (1975).

^kThis study.

^lTaenite is paramagnetic at room temperature for Ni < 30 wt%.

spectroscopy. The situation for the most unequilibrated ordinary chondrites is somewhat different because their peak metamorphic temperatures below 400 °C prevented the formation of tetrataenite and preserved martensite, which would otherwise have decomposed into plessite (like in equilibrated chondrites).

The intrinsic magnetic properties of the FeNi minerals found in ordinary chondrites are summarized in Table 2. Because B_C , B_{CR} , and M_{RS} values depend closely on the magnetic domain state and hence the microstructure in which the minerals are found, these values are not given in Table 2. For instance, tetrataenite grains within plessite have lower coercivity than the

smaller tetrataenite grains in the cloudy zone (Uehara et al. 2011), and measured B_{CR} values for tetrataenite in meteorites range from 77 mT (Funaki et al. 1986) to approximately 1000 mT (Uehara et al. 2011) on large grains (approximately 500 μm) extracted from Toluca iron meteorite and on the cloudy zone of Ausson L5 and Agen H5 chondrites, respectively. Similarly, measured B_C values for kamacite range from 1 mT (Nagata et al. 1975) to 600 mT (Lappe et al. 2011) for a EH3 chondrite and on a synthetic dusty olivine, respectively. As a general rule for ordinary chondrites, tetrataenite stands out with a much higher coercivity and saturation remanence (Funaki et al. 1986; Nagata et al. 1986, 1991; Uehara

et al. 2011) than kamacite and martensite that are characterized by low coercivity and low saturation remanence (Nagata et al. 1975; Wasilewski 1981) consistent with their multidomain state. Indeed, the magnetic single-domain size for kamacite, which is controlled by shape anisotropy for nearly all grain elongations, is restricted to a very narrow range: approximately 20–50 nm and approximately 17–22 nm for grains with axial ratios of 0.5 and 0.8, respectively (Butler and Banerjee 1975). By comparison, the critical size below which tetrataenite becomes superparamagnetic is 7 nm at room temperature (Nagata et al. 1991). The single-domain grain-size range for tetrataenite is presently unknown, but can be constrained on the basis of its grain-size independent (intrinsic) magnetic material parameters. According to Néel et al. (1964) and Paulevé et al. (1968), the magnetocrystalline anisotropy constant K is $1.0\text{--}1.3 \times 10^6 \text{ J m}^{-3}$ and the saturation magnetization M_S is $1.3 \times 10^6 \text{ A m}^{-1}$. With these values, we obtain 1.5 to 2 T for the microcoercivity $\mu_0 H_k = 2K/M_S$ and 0.94–1.22 for the dimensionless magnetic hardness parameter $Q = K/K_d$, where $K_d = \frac{1}{2}\mu_0 M_S^2$ is the scale for the stray field energy. According to Rave et al. (1998), the single-domain state in equidimensional particles with $Q = 0.94\text{--}1.22$ is stable to an edge length of at least $L_{\min} = 20$ to $23 L_{\text{ex}}$, where L_{ex} is the exchange length with $L_{\text{ex}} = \sqrt{A/K_d}$, and A is the exchange constant, which for the tetragonal (L1₀) Fe_{0.5}Ni_{0.5} alloy is not available, but can be approximated by that of disordered Fe_{0.5}Ni_{0.5} $A = 15.5 \times 10^{-11} \text{ J m}^{-1}$ (e.g., Hennemann and Siegel 1976). Thus, with $L_{\text{ex}} = 3.8 \text{ nm}$, the single-domain state is the energetically most stable magnetization configuration in particles with grain sizes up to at least $L_{\min} = 77\text{--}89 \text{ nm}$. Depending on the magnetization history, the single-domain state may exist as a metastable state well beyond L_{\min} . This is in agreement with micromagnetic simulations of the cloudy zone showing that tetrataenite islands up to approximately 100 nm in diameter have a single-domain behavior (Bryson et al. 2014).

RESULTS AND DISCUSSION

Spatial Homogeneity of Hysteresis Properties

We tested the consistency of hysteresis properties in a given meteorite by measuring multiple fragments for some meteorites. The data indicate that B_{CR} , B_C , and M_{RS}/M_S have well-defined values for a given meteorite even for small samples down to a few tens mg (Fig. 2). This remains true even for LL chondrites that have low metal concentration and high magnetic anisotropy (see Anisotropy Effects section). For example, we measured the hysteresis properties of 16 samples of the Boursour

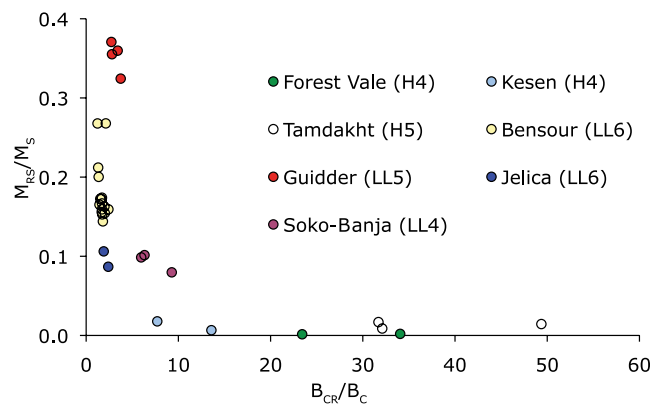


Fig. 2. Hysteresis properties for multiple samples of selected meteorites.

meteorite and these properties are constant for masses as low as 20 mg. However, because of the possible presence of a discrete number of large metallic grains, for small samples (a few tens of mg), M_{RS} , M_S , and χ can show strong departures from the mean value, especially in metal-poor LL chondrites (see, e.g., Gattacceca et al. 2003). Like bulk susceptibility (Rochette et al. 2003) or anisotropy of magnetic susceptibility (Gattacceca et al. 2005), hysteresis properties are representative intrinsic properties of a given ordinary chondrite at the scale of a few tens of mg. However, in LL chondrites, reliable estimates of M_{RS} and M_S require masses above 100 mg.

The consistency of hysteresis properties within a given meteorite enables merging results from multiple samples of the same meteorite. Merged values were computed in the following way: M_{RS} and M_S were mass-weighted, B_C was M_S -weighted (giving similar results to the approach of Nagata and Funaki [1982] for computing B_C for a mixture of two ferromagnetic materials), and B_{CR} were M_{RS} -weighted. This ensures that the mean values are equal to what would have been measured had the different samples been combined for a single measurement. The results, averaged at the meteorite level, are given in Table 3.

Hysteresis Properties in Different Ordinary Chondrite Classes

The hysteresis properties of H and L chondrites are broadly similar, with low M_{RS}/M_S and high B_{CR}/B_C (Table 4, and representative cycles provided in Fig. 1). Together with the curvature observed on the hysteresis cycles up to 0.7 T (due to the high demagnetizing field of multidomain kamacite), these values show that soft multidomain FeNi metal (in the form of mostly kamacite and with a possible small contribution from taenite with >30 wt% Ni in some unusual cases)

Table 3. Hysteresis properties of ordinary chondrites and HED achondrites.

Meteorite	Shock ^b	mass ^a (g)	B_C (mT)	B_{CR} (mT)	M_S (Am ² kg ⁻¹)	M_S (Am ² kg ⁻¹)	B_{CR}/B_C	M_{RS}/M_S	χ_{HF} m ³ kg ⁻¹	χ_f m ³ kg ⁻¹	M_S/χ_f $\times 10^5$ A m	References
Asco	H6		9.79	178.6			18.24	1.92E-02				d
Agen	H5	0.093	2.34	176.0	33.91	4.42E-01	75.37	1.30E-02	6.54E-06	1.91E-04	1.78	d
Bath	H4		1.47	41.9	40.33	4.67E-01	28.50	1.16E-02				e
Blansko	H6	0.279	0.43	5.0	43.66	2.81E-01	11.57	6.44E-03	1.82E-07			d
Chergach	H5	0.638	1.75	54.3	35.71	2.62E-01	30.98	7.34E-03	6.19E-06	1.75E-04	2.04	d
Collescipoli	H5		1.65	95.6	42.87	5.38E-01	57.94	1.25E-02				e
Dhajala	H3.8	0.121	2.14	63.6	40.28	2.78E-01	29.72	6.90E-03	4.88E-06	1.27E-04	3.16	d
Djati-Pengilon	H6	0.149	4.18	335.0	33.42	5.17E-01	80.16	1.55E-02	5.01E-06	1.29E-04	2.58	d
Forest City	H5		2.30	33.9	22.31	4.57E-01	14.74	2.05E-02				e
Forest Vale	H4	0.068	0.30	9.0	42.16	6.35E-02	30.05	1.51E-03	5.47E-06	2.10E-04	2	d
Gursum ^e	H4/5	0.107	2.32	225.8	28.88	2.61E-01	97.29	9.05E-03	4.05E-06	1.05E-04	2.76	d
Hainaut	H3-6		0.50	3.1	41.40	3.29E-01	6.20	7.96E-03				e
Jilin	H5		1.62	82.5	37.51	4.95E-01	50.93	1.32E-02				e
Kernouvé	H6	0.067	1.00	84.4	49.01	3.20E-01	84.11	6.53E-03	6.00E-06	2.98E-04	1.64	d
Kesen	H4		0.82	8.7	49.64	5.15E-01	10.61	1.04E-02				e,f
Lançon	H6	0.085	0.66	5.4	47.27	2.43E-01	8.19	5.15E-03	6.36E-06	3.12E-04	1.52	d
Mount Browne	H6		1.25	85.7	43.43	5.00E-01	68.56	1.15E-02				e
Ochansk	H4	0.122	1.27	42.2	52.10	3.80E-01	33.14	7.29E-03	7.58E-06	2.93E-04	1.78	d
Pantar	H5	0.043	1.81	62.8	34.78	3.59E-01	34.75	1.03E-02	5.88E-06			d
Phum Sambo	H4	0.060	1.02	22.2	48.93	3.35E-01	21.68	6.84E-03	8.00E-06	3.85E-04	1.27	d
Plainview (1917)	H5		1.90	18.5	33.56	5.36E-01	9.74	1.60E-02				e
Pultusk	H5	0.067	1.03	26.8	48.14	3.03E-01	25.93	6.29E-03	6.00E-06	2.20E-04	2.18	d
Sie. Marguerite	H4	0.480	0.35	9.2	40.46	6.20E-02	25.87	1.53E-03	5.25E-06	1.75E-04	2.31	d
Tamdakht	H5	0.427	1.81	79.1	38.68	3.79E-01	43.79	9.79E-03	1.23E-06	1.75E-04	2.21	d
Trenzano	H3/4	0.089	0.73	57.3	42.70	3.23E-01	78.56	7.56E-03	5.75E-06	2.96E-04	1.44	d
Bremervörde	H/L3.9	1.290	2.25	55.40	15.12	1.42E-01	24.66	9.40E-03	9.73E-06	9.82E-05	1.54	d
Tieschitz	H/L3.6	0.020	7.67	102.80	16.79	3.59E-01	13.40	2.14E-02	3.14E-06	5.59E-05	3.00	d
Alfianello	L6	0.127	0.52	10.8	14.54	2.86E-02	20.61	1.97E-03	1.89E-06	7.50E-05	1.94	d
Ausson	L5	0.066	9.40	289.8	11.10	4.48E-01	30.83	4.03E-02	1.75E-06	6.10E-05	1.82	d
Barwell	L5	0.580	8.53	321.0	15.37	4.26E-01	37.62	2.77E-02	2.70E-06	7.13E-05	2.16	d
Baszkówka	L5				10.77	6.46E-02	14.00	7.14E-03				h
Braunschweig	L6	0.733	1.70	31.2	17.65	7.06E-02	18.37	4.00E-03		5.62E-05	3.14	d
Buschhoff	L6		1.60	32.0	21.18	1.71E-01	20.00	8.06E-03				e
Château-Renard	L6	0.106	0.64	18.2	12.44	3.89E-02	28.50	3.13E-03	1.39E-06	5.55E-05	2.24	d
Fisher	L6	0.039	0.32	8.8	17.16	3.84E-02	27.13	2.24E-03	2.87E-06	8.93E-05	1.92	d
Fukutomi	L5		2.04	50.0	30.11	7.14E-01	24.51	2.37E-02				f
Hallingeberg	L3	0.027	3.91	51.5	23.83	3.41E-01	13.17	1.43E-02	2.41E-06	7.49E-05	3.18	d
Hedjaz	L3.7-6	0.093	3.20	53.3	13.22	1.46E-01	16.67	1.10E-02	2.53E-06	4.35E-05	3.04	d
Homestead	L5	0.129	6.10	181.1	13.61	3.46E-01	29.70	2.54E-02	1.95E-06	2.87E-05	4.75	d

Table 3. *Continued.* Hysteresis properties of ordinary chondrites and HED achondrites.

Meteorite	Shock ^b	mass ^a (g)	B_C (mT)	B_{CR} (mT)	M_S (Am ² kg ⁻¹)	M_S (Am ² kg ⁻¹)	B_{CR}/B_C	M_{RS}/M_S	χ_{HF} m ³ kg ⁻¹	χ_f m ³ kg ⁻¹	M_S/χ_f $\times 10^5$ A m	References
Lanzenkirchen	L4		1.04	13.2	25.92	1.87E-01	12.69	7.22E-03				e
Jalu	L6	3	1.21	21.8			18.01	4.19E-03				d
Kendleton	L4	3	0.024	4.14	12.05	2.22E-01	13.05	1.84E-02	1.72E-06	3.15E-05	3.83	d
Khojar	L3.6	4	0.057	3.82	24.00	3.64E-01	7.75	1.52E-02	1.66E-06	1.19E-04	2.02	d
L'Aigle	L6	3	0.146	6.64	17.34	3.53E-01	33.92	2.03E-02	4.76E-06	8.61E-05	2.01	d
Marmande	L5	3	0.070	11.37	13.80	4.13E-01	24.52	2.99E-02	2.68E-06	4.75E-05	2.91	d
Mező-Madaras	L3.7	3	0.059	3.34	17.27	2.21E-01	8.36	1.28E-02	2.44E-06	4.89E-05	3.53	d
Monte Milone	L6	3	0.600	13.36	9.18	4.98E-01	22.34	5.42E-02	2.32E-06	6.49E-05	1.42	d
Mount Tazerzait	L5	1	0.095	0.86	13.98	5.10E-02	18.58	3.65E-03	1.50E-06	6.81E-05	2.05	d
Paranaíba	L6	6	0.417	1.49	15.87	1.04E-01	14.64	6.56E-03	2.41E-06	1.03E-04	1.54	d
Pè	L6	1	0.033	10.83	8.33	2.97E-01	41.79	3.57E-02	1.39E-06	2.77E-05	3.01	d
Saratov	L4	2	0.075	3.54	23.09	3.77E-01	41.21	1.63E-02	4.05E-06	9.68E-05	2.39	d
Sevrukovo	L5		3.40	18.5	19.66	3.91E-01	5.44	1.99E-02				e
St. Chinian	L6		0.726	9.48	13.27	3.37E-01	23.12	2.54E-02	1.62E-06	4.27E-05	3.11	d
Tadjera	L5	6	0.117	0.69	23.46	6.94E-02	20.09	2.96E-03	2.82E-06	1.04E-04	2.26	d
Tennasilim	L4	2	0.500	5.30	28.34	6.83E-01	27.36	2.41E-02				e
Tourinnes la Grosse	L6	3	0.063	7.83	16.70	4.44E-01	37.69	2.66E-02	4.19E-06	1.01E-04	1.66	d
Tuan Tuc	L6	5	0.050	0.85	32.75	1.24E-01	16.60	3.79E-03	4.19E-06	1.64E-04	2.00	d
Utrecht	L6	2	0.076	4.59	19.92	4.72E-01	63.69	2.37E-02	2.19E-06	6.48E-05	3.08	d
Albareto	L/LL4	3	3.080	8.19	198.9	1.95E-01	24.27			3.52E-05		d
Bishunpur	L/LL3.1	1	0.062	5.31	63.0	3.81E-01	11.85	2.24E-02	2.08E-06	6.55E-05	2.34	d
Bjurböle	L/LL4	1	0.112	1.40	20.55	4.46E-01	111.32	2.17E-02	2.18E-06			d
Cabezo de Mayo	L/LL6		0.101	3.13	23.87	3.69E-01	61.67	1.55E-02	4.65E-06	1.49E-04	1.33	d
Knyhinya	L/LL5		0.161	0.36	8.57	2.24E-02	45.11	2.62E-03	1.29E-06	4.65E-05	1.84	d
Adzi-Bogdo	LL3-6	2	0.089	22.11	91.57	1.80E-01	4.14	5.56E-02	1.30E-06	8.30E-06	3.89	d
Alta 'Ameem	LL5		0.500	56.00	217.00	5.36E-01	3.88	2.00E-01				e
Appley Bridge	LL6	3		16.00	47.00	1.21E-01	2.94	5.88E-02				g
Benares (a)	LL4		0.032	12.28	265.70	4.14E-01	21.64	4.10E-02	1.61E-06	3.96E-05	2.55	d
Benguerir	LL6	3	0.059	26.35	153.90	4.31E-01	5.84	8.17E-02	1.47E-06	1.45E-05	3.65	d
Bensour	LL6	3	4.383	40.82	60.44	5.11E-01	1.48	1.55E-01	2.11E-06	3.05E-06	10.81	d
Champur	LL3.5	1	1.644	8.86	91.79	2.01E-01	10.36	2.97E-02	1.48E-06	2.87E-05	2.36	d
Douar Mghila	LL6		0.102	64.53	167.75	9.42E-01	2.60	1.67E-01	1.92E-06	1.19E-05	4.73	d
Dhurmsala	LL6	3	0.500	11.90	125.00	2.04E-01	10.50	5.52E-02				e
Guidder	LL5	3	1.788	135.23	414.47	7.69E-01	3.06	2.36E-01	1.03E-06	1.38E-05	2.36	d
Jelica	LL6	3	0.690	26.07	51.91	7.20E-02	1.99	7.78E-02	6.09E-07	3.18E-06	2.91	d
Kilabo	LL6	3	1.036	81.08	137.08	6.11E-01	1.69	2.25E-01	1.78E-06	3.32E-06	8.17	d
Konevo	LL5		1.461	56.47	171.10	5.82E-01	3.03	1.44E-01	1.30E-06	8.56E-06	4.73	d
Krymka	LL3.1	3	0.594	21.88	62.35	3.06E-01	2.85	8.47E-02	8.88E-07	1.89E-05	1.91	d
Manbhoom	LL6	3	1.170	26.01	51.96	1.57E-01	2.00	8.90E-02	1.40E-06	1.29E-06	13.72	d

Table 3. *Continued.* Hysteresis properties of ordinary chondrites and HED achondrites.

Meteorite	Shock ^b	mass ^a (g)	B_C (mT)	B_{CR} (mT)	M_S (Am ² kg ⁻¹)	M_S (Am ² kg ⁻¹)	M_S (Am ² kg ⁻¹)	B_{CR}/B_C	M_{RS}/M_S	χ_{HF} m ³ kg ⁻¹	χ_f m ³ kg ⁻¹	M_S/χ_f $\times 10^5$ A m	References
Ngawi	LL3.6	0.500	14.74	49.88	2.51	1.54E-01	1.54E-01	3.38	6.16E-02	5.07E-07	1.45E-05	1.73	d
Nyirabrany	LL5	0.500	41.30	330.00	5.81	7.35E-01	7.35E-01	7.99	1.26E-01				c
Olivenza	LL5	0.430	68.37	240.34	3.77	5.83E-01	5.83E-01	3.52	1.54E-01	1.31E-06	1.37E-05	2.76	d
Oued el Hadjar	LL6	0.560	60.05	180.62	4.67	9.19E-01	9.19E-01	3.01	1.97E-01	2.14E-06	9.28E-06	5.03	d
Parnallee	LL3.6	0.070	12.13	125.40	8.04	2.25E-01	2.25E-01	10.34	3.02E-02	2.25E-06	2.68E-05	3.00	d
Saint-Séverin	LL6		52.00	184.00	3.33	5.00E-01	5.00E-01		1.50E-01				g
Savitschenskoe	LL4	0.190	1.54	34.47	6.91	4.23E-02	4.23E-02	22.37	6.13E-03	1.04E-06	3.79E-05	1.82	d
Semarkona	LL3.0	0.026	17.05	45.50	5.49	5.67E-01	5.67E-01	2.67	1.03E-01	8.34E-07	2.06E-05	2.66	d
Siena	LL5	0.057	28.55	133.00	4.37	3.16E-01	3.16E-01	4.66	7.23E-02	1.55E-06	9.95E-06	4.39	d
Soko-Banja	LL4	0.237	31.14	194.34	5.93	5.08E-01	5.08E-01	6.24	8.56E-02	1.68E-06	1.25E-05	4.76	d
Tuxtucac	LL5		4.00	25.50	3.49	5.50E-02	5.50E-02	6.38	1.58E-02				g
Uden	LL7 ^c	0.185	61.79	101.10	0.46	8.57E-02	8.57E-02	1.64	1.86E-01	6.00E-07	7.90E-07	5.83	d
Vavilovka	LL6	0.500	21.00	62.50	1.33	1.07E-01	1.07E-01		8.01E-02				e
HED													
Bereba	Eucrite	0.729	3.16		6.53E-02	8.29E-04	8.29E-04		1.21E-02	3.53E-07	3.43E-07	1.90	d
Bouvante	Eucrite	0.835	2.20	14.54	4.97E-02	5.09E-04	5.09E-04	6.61	1.02E-02	4.49E-07	3.49E-07	1.43	d
Juvinas	Eucrite	0.507	1.56	33.26	2.70E-01	1.72E-03	1.72E-03	21.35	6.35E-03	4.18E-07	9.93E-07	2.72	d
Pasamonte	Eucrite	0.073	5.06	33.92	8.22E-02	9.68E-04	9.68E-04	6.70	1.18E-02	4.54E-07	3.10E-07	2.65	d
Manegaon	Diogenite	0.494	1.03	17.90	1.45E-01	5.27E-04	5.27E-04	17.37	3.64E-03	2.88E-07	1.23E-06	1.18	d
Roda	Diogenite	0.498	10.35	58.50	2.59E-02	7.78E-04	7.78E-04	5.65	3.00E-02	3.16E-07	8.34E-08	3.10	d
Shalka	Diogenite	0.905	4.03	84.43	1.17E-01	9.44E-04	9.44E-04	20.96	8.08E-03	3.69E-07	2.66E-07	4.39	d
Chaves	Howardite	0.181	4.17	142.20	1.00E-02	3.38E-04	3.38E-04	34.09	3.37E-02	4.32E-07			d
Le Teilleul	Howardite	0.217	1.64	36.02	3.17E-01	1.65E-03	1.65E-03	22.00	5.21E-03	4.27E-07	1.14E-06	2.78	d
Pavlovka	Howardite	0.296	1.40	9.56	4.09E+00	2.76E-02	2.76E-02	6.82	6.76E-03	7.22E-07	3.34E-05	1.22	d

^aSample mass is not given in a number of previous studies.

^bShock stage as defined by Stöffler et al. (1991).

^cUden (LL7) has been merged with LL6 for the mean in Table 3. Gursum (H4/5) results have been merged with H5 in Table 3, also based on the proposed H5 reclassification (Schultz et al. 1990).

^dThis study.

^eTerho et al. (1992).

^fNagata and Sugiura (1976).

^gNagata et al. (1986).

^hKrol and Lang (1996).

See text for definition of magnetic parameters.

Table 4. Mean hysteresis properties by meteorite class, metamorphic type, and shock stage.

	N	B_C (mT)	SD	B_{CR} (mT)	SD	M_S (Am ² kg ⁻¹)	SD	M_{RS}^b (Am ² kg ⁻¹)	SD	N	M_{RS}	B_{CR}/B_C	SD	M_R/M_S	SD	$M_S/\tau_r \times 10^5$ A m	SD	FD (%)
H	25	1.78	1.84	72.3	78.2	40.46	6.99	0.354	0.123	30	39.1	26.8	9.76E-03	4.65E-03	2.05	0.52	1.4 ± 1.1	
H/L	2	4.96	2.71	79.1	23.7	15.95	0.84	0.251	0.108	2	19.0	5.6	1.54E-02	5.98E-03	2.27	0.73	1.6 ± 0.8	
L	31	5.62 ^a	3.72	162.4 ^a	133.0	17.93	6.09	0.347 ^a	0.164 ^a	22	25.90 ^a	12.2	2.18E-2 ^a	1.22E-02	2.54	0.80	0.5 ± 0.7	
L/LL	5	3.68	2.81	125.3	73.0	17.51	5.69	0.283	0.154	5	50.8	34.7	1.55E-02	7.93E-03	1.84	0.41	1.1 ± 1.7	
LL	28	36.40	28.64	136.3	92.9	4.11	2.15	0.387	0.223	32	5.8	5.4	1.06E-01	6.39E-02	4.46	2.99	0.4 ± 0.5	
H3	2	1.44	0.71	60.4	3.2	41.49	1.21	0.300	0.022	2	54.1	24.4	7.23E-03	3.29E-04	2.30	0.86		
H4	6	0.87	0.44	22.2	14.8	45.91	4.58	0.321	0.166	9	24.8	7.4	6.41E-03	3.90E-03	1.86	0.39		
H5	10	1.85	0.38	84.7	63.5	35.69	6.73	0.385	0.099	13	43.7	25.9	1.18E-02	4.05E-03	2.20	0.32		
H6	6	1.83	3.33	115.7	114.3	43.36	5.41	0.352	0.113	6	45.1	32.9	1.07E-02	5.21E-03	1.93	0.59		
L3	3	3.69	0.25	36.3	10.8	21.70	3.13	0.309	0.063	3	9.8	2.4	1.31E-02	9.02E-04	3.12	0.69		
L4	4	3.51	1.56	89.6	57.8	22.35	6.23	0.303	0.217	4	23.6	11.8	1.59E-02	5.83E-03	3.17	0.71		
L5	8	5.96 ^a	3.70 ^a	165.0 ^a	125.4 ^a	16.42	5.66	0.356 ^a	0.201 ^a	8	23.2 ^a	9.6 ^a	2.20e-2 ^a	1.12e-2 ^a	2.80	1.19		
L6	14	7.70 ^a	3.74 ^a	257.8 ^a	119.8 ^a	16.64	5.89	0.365 ^a	0.089 ^a	7	34.5 ^a	14.5 ^a	2.72e-2 ^a	1.40e-2 ^a	2.26	0.62		
L S1	3	5.20	4.17	173.4	198.0	14.74	5.66	0.188	0.132	4	21.9	11.7	1.52E-02	1.24E-02	2.75	0.50		
L S2	3	4.48	0.72	194.4	69.1	23.79	3.47	0.511	0.128	3	44.1	15.0	2.14E-02	0.36E-02	2.73	0.35		
L S3	6	7.19	3.70	211.3	121.0	14.49	3.19	0.398	0.090	7	27.0	10.3	2.66E-02	1.55E-02	2.10	0.68		
L S4	5	3.28	1.65	65.4	58.5	18.34	4.20	0.158	0.103	10	18.5	7.0	1.23E-02	0.68E-02	3.32	1.11		
L S5	4	0.58	0.19	13.0	3.6	19.22	7.99	0.054	0.035	5	23.2	4.8	2.78E-03	0.72E-03	2.02	0.13		
L S6	2	1.09	0.40	17.8	4.0	19.67	3.79	0.087	0.017	2	17.4	2.7	4.76E-03	1.80E-03	1.90	0.36		
LL3	5	14.88	4.42	75.0	29.9	5.28	2.02	0.291	0.146	5	5.9	3.6	6.26E-02	3.02E-02	2.48	0.40		
LL4	3	14.99	12.23	164.8	96.7	7.82	2.02	0.321	0.201	3	16.4	7.2	4.05E-02	2.87E-02	3.09	1.23		
LL5	7	55.70	37.99	218.8	118.4	3.92	0.92	0.522	0.218	8	4.7	1.7	1.32E-01	6.48E-02	3.28	0.57		
LL6	12	38.73	21.57	111.1	54.0	3.16	1.51	0.404	0.278	13	3.5	2.6	1.21E-01	5.42E-02	7.05	3.79		

^aIncludes only meteorites with shock stage < S4 (see text).^bIncludes data from Rochette et al. (2003) except Nadiabondi that was described as a weathered specimen.

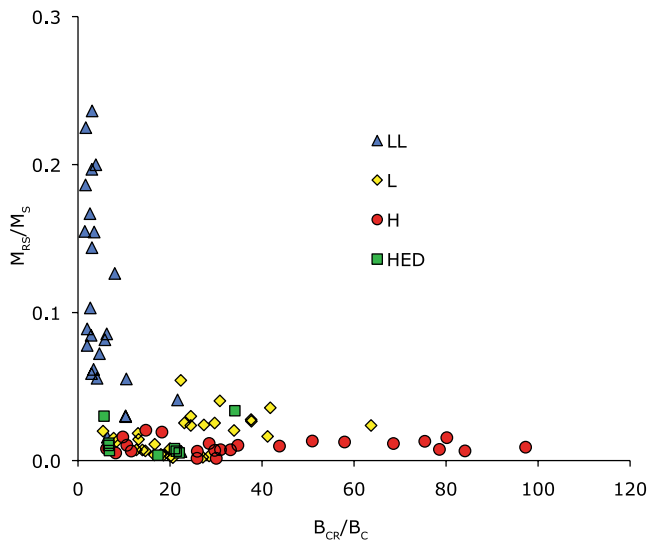


Fig. 3. Hysteresis properties for ordinary chondrites and HED. Each circle corresponds to one meteorite.

dominates the hysteresis properties. Conversely, LL chondrites stand out with higher M_{RS}/M_S and lower B_{CR}/B_C , with almost no overlap with H and L chondrites (Fig. 3). Along with the “wasp-waisted” shape of their hysteresis loops, this is attributable to the higher tetraenaite contribution to hysteresis properties in these meteorites, as previously observed (Nagata and Funaki 1982; Nagata 1988; Pesonen et al. 1993; Gattacceca et al. 2003). In L chondrites, the existence of samples with $M_{RS}/M_S > 0.02$ and B_{CR}/B_C of 20–40 that are outside of the theoretical zone for multidomain grains reflects the significant contribution of tetraenaite

to the hysteresis properties (Fig. 3). This is also visible in the “wasp-waistedness” of their hysteresis loops, although this is less pronounced than in LL chondrites (Fig. 1). L/LL and H/L chondrites have hysteresis properties broadly similar to L and H chondrites.

As expected, H, L, and LL chondrites have distinct ranges for M_S (Fig. 4a). This stems from their different bulk metal abundances that is the basis of the definition of these groups and which also clearly controls their magnetic susceptibility measurements (Rochette et al. 2003). The mean M_S values for H, L (Table 4) correspond to a minimum metal content of 18.0 ± 3.1 and 8.0 ± 2.7 , respectively, based on the simplistic assumption that all the metal is in the form of kamacite with $M_S = 224 \text{ Am}^2 \text{ kg}^{-1}$. These values are lower limits because tetraenaite has a lower M_S than kamacite, and paramagnetic taenite does not contribute to M_S . They compare well with the Fe + Ni + Co abundances obtained from chemical analyses of the metallic fraction of meteorites (computed from the data of Jarosewich [1990] by selecting falls only, excluding meteorites described as weathered by the author, using updated classifications for some meteorites, and discarding values more than 3 SD away from the mean value for H and L chondrites): $18.2 \pm 1.4 \text{ wt}\%$ ($n = 25$) for H and $8.5 \pm 0.8 \text{ wt}\%$ ($n = 53$) for L (Table 1).

Although they have distinct ranges for M_S , it is noteworthy that H, L, and LL chondrites have similar ranges for M_{RS} (Fig. 4b and 5), as already noticed on a more limited M_{RS} database by Rochette et al. (2003). The observation in Rochette et al. (2003) that H chondrites have lower M_{RS} scatter than L and LL

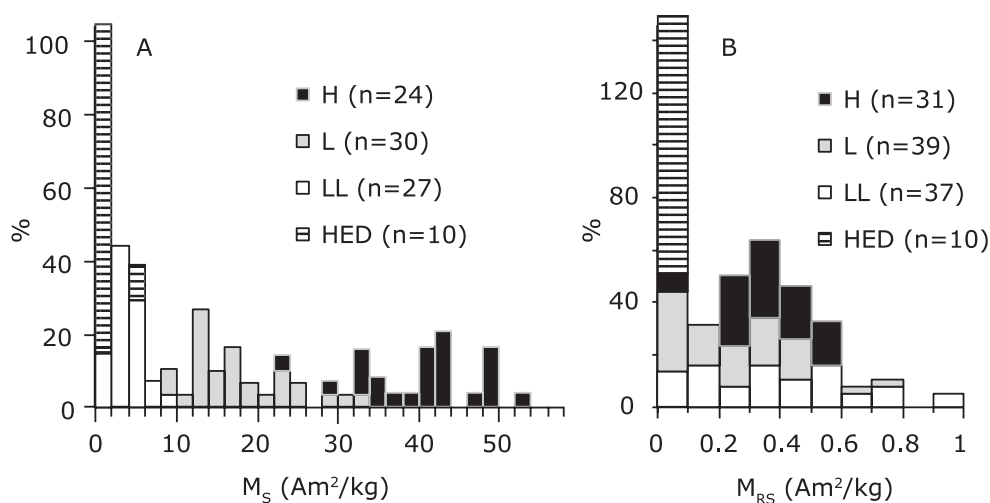


Fig. 4. Frequency histograms of M_S and M_{RS} for LL, L, H chondrites, and HED achondrites. The percentages are computed within each group. The number of data for each class is indicated between parentheses. The M_{RS} histogram includes data from Rochette et al. (2003).

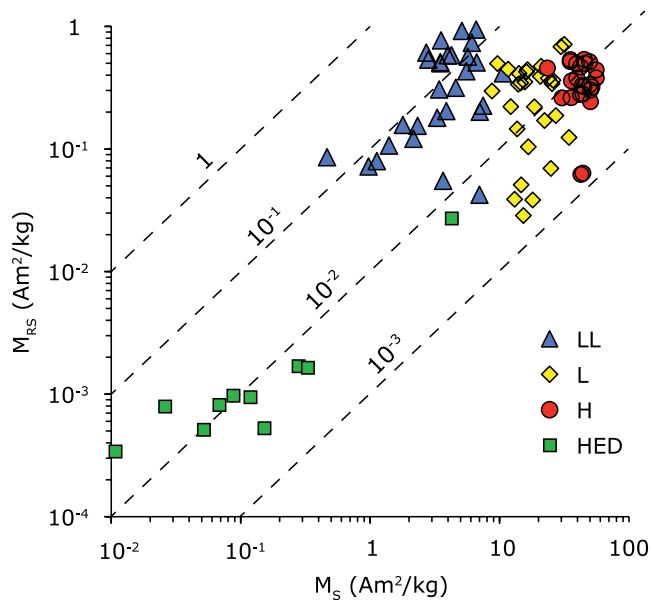


Fig. 5. M_{RS} versus M_S for H, L, LL, and HED meteorites. The dotted lines are lines of constant M_{RS}/M_S .

is also confirmed, as well as the possible existence of two clusters for H chondrites with a gap of M_{RS} values in the $0.38\text{--}0.44\text{ Am}^2\text{ kg}^{-1}$ interval in our database, these two groups being undistinguishable in terms of petrographic type or shock stage. The smaller scatter observed for H chondrites is due at least in part to their higher metal concentration that enables more accurate bulk measurements compared with L and LL chondrites for samples of similar size. The absence of correlation between M_{RS} and M_S within each class (Fig. 5) confirms the strong decoupling between induced and remanent magnetic properties in ordinary chondrites.

It is noteworthy that HED achondrites do not follow the same trend (Fig. 5, Table 3). For an equivalent M_S , they have much lower M_{RS} , in agreement with the usual absence of taenite and tetrataenite (e.g., Mayne et al. 2009). Moreover, HEDs show a reasonably linear relationship between M_{RS} and M_S (Fig. 5), indicating that the same mineral controls the remanent and the induced magnetic properties. This mineral, multidomain kamacite, varies only in concentration. This was already indicated by the good correlation between M_{RS} and magnetic susceptibility in HED meteorites (Rochette et al. 2009) and lunar rocks (Rochette et al. 2010).

χ_{HF} average values for H, L, LL, and HED are the following: 5.3 ± 2.0 , 2.8 ± 0.9 , 1.4 ± 0.5 , and $0.4 \pm 0.6\ 10^{-6}\text{ m}^3\text{ kg}^{-1}$. This apparent trend with chondrite class is clearly an artifact of incomplete removal of the ferromagnetic slope, as the paramagnetic contribution

should increase from H to LL chondrites in view of the increasing Fe content of the silicates. Only the HED values provide a significant estimate of the true paramagnetic contribution that is in good agreement with the theoretical value of $0.35 \times 10^{-6}\text{ m}^3\text{ kg}^{-1}$ that can be computed from the elemental composition of these meteorites (see discussion in Gattacceca et al. 2008).

First-Order Reversal Curve Properties

We measured the first-order reversal curve (FORC) properties of three chondrites: Gudder (LL5), Chergach (H5), and Tamdakht (H5). Despite the strong differences between hysteresis loops for H and LL chondrites (Fig. 1), their FORC diagrams share the same distinct features (Fig. 6). This strongly suggests the presence of the same magnetic phases with different mixing ratios. Three distinct features are apparent, which are most pronounced in Gudder: (1) a high-coercivity ridge running parallel to the B_C axis with some small offset toward positive bias field; (2) a low-coercivity ($B_C < 100\text{ mT}$) contribution, which is also offset toward positive bias field by a few tens of mT; and (3) a diagonally running positive ridge with a negative trough attached to its right, both extending from the low-coercivity maximum at an angle of about 45° from the B_C axis down to negative bias field. This distinct set of FORC features has already been observed by Acton et al. (2007) in chondrules of the Bjurböle L/LL4 chondrite. Acton et al. (2007) ascribed the diagonal ridge to interactions between a very low-coercivity (“nearly superparamagnetic”) component and a magnetically hard component. We also interpret the diagonal ridge in terms of interactions between hard and soft components, but suggest that the coercivity of the magnetically soft component (kamacite) needs not be low in absolute terms, but just distinctly lower than that of the magnetically hard phase (tetrataenite) in order for both components to have a mutual biasing effect. The simplest way to demonstrate the presence of interactions is by way of feature (2). Here, the shift of the low-coercivity distribution toward positive bias field represents “earlier” downswitching of the soft component along the descending major hysteresis branch (at a reversal field that is smaller than the switching field of the soft component when isolated), and delayed upswitching along the FORC, i.e., the soft component is destabilized by the presence of the stray fields from the hard component. Premature downswitching and delayed upswitching reflect demagnetizing interactions, which are also reflected by the fact that IRM acquisition requires higher fields than demagnetization of the saturation remanence does

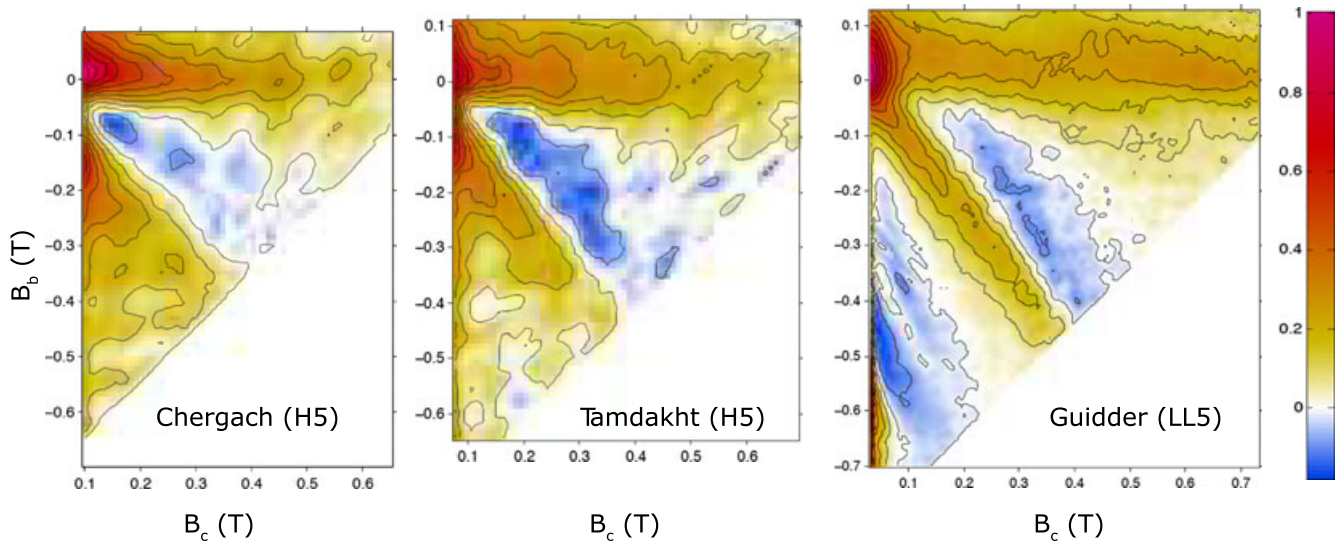


Fig. 6. First-order reversal curve diagrams. To better bring out the high-coercivity part of Chergach and Tamdakht, which are dominated by viscous contributions, their FORC diagrams were truncated at the low-coercivity side.

(Cisowski-Wohlfarth R values are 0.25 for Gudder and 0.15 for the Tamdakht sample). The magnetic interactions between kamacite and tetrataenite had already been observed at microscopic scale in H ordinary chondrites scale by magneto-optical imaging (Uehara et al. 2011).

Hysteresis and Susceptibility

Ferromagnetic susceptibility and M_S are well correlated for all three classes of ordinary chondrites (Fig. 7). The M_S/χ_f ratios are 1.83×10^5 , 2.54×10^5 , and 3.77×10^5 A m in H, L, and LL chondrites, respectively (Table 4). This illustrates again the dichotomy between H and L chondrites, and LL chondrites. In H and L chondrites, the induced magnetic properties are most likely controlled by multidomain kamacite, although some influence of tetrataenite is already visible in the L group. However, the M_S/χ value in H and L chondrites (overall mean value is 2.32×10^5) is significantly lower than the theoretical $M_S/\chi = 4.12 \times 10^5$ A m obtained using $M_S = 224 \text{ Am}^2 \text{ kg}^{-1}$ for kamacite (Crangle and Hallam 1963) and $\chi = 5.44 \times 10^{-4} \text{ m}^3 \text{ kg}^{-1}$ determined for multidomain iron spheres (Rochette et al. 2009). The discrepancy is even stronger if one takes into account that part of the metal is in the form of tetrataenite that has likely a higher M_S/χ than kamacite (see discussion in Rochette et al. [2003] about the magnetic susceptibility of tetrataenite).

This deviation can be attributed to three factors that can increase apparent susceptibility: the presence of superparamagnetic grains and/or the presence of

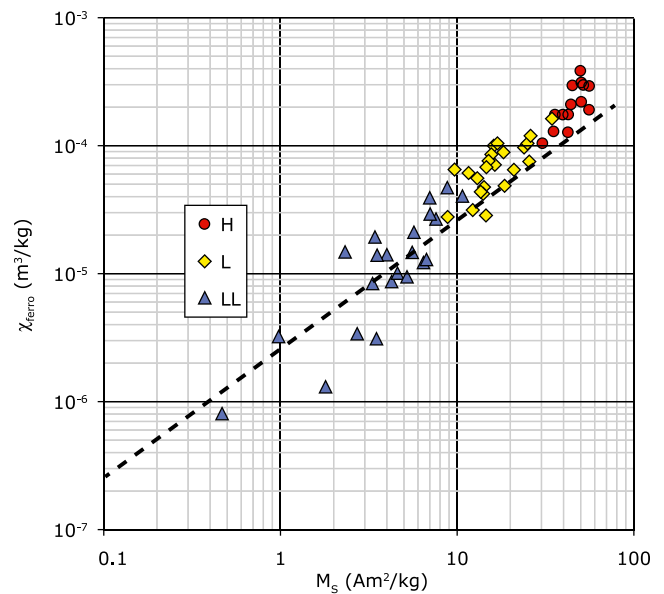


Fig. 7. χ_f versus M_S for the three classes of ordinary chondrites. The two properties are measured on the same sample. The dotted line is the theoretical line for multidomain kamacite (see text).

elongated metallic grains, and/or magnetic interactions. Indeed, superparamagnetic metal grains can have a magnetic susceptibility up to 10 times that of multidomain grains (see, e.g., Van de Moortèle et al. 2007). We tested for the presence of superparamagnetic FeNi grains (i.e., with a size below about 20 nm for kamacite [Dunlop and Özdemir 1997] and 7 nm for tetrataenite [Nagata et al. 1991]), by measuring the frequency dependence of low-field susceptibility of

Table 5. FeNi grain shapes in ordinary chondrites.

Meteorite		Median aspect ratio	Mean aspect ratio	SD	<i>n</i>
Baszkówka	L5	1.87	1.99	0.55	2873
Estacado	H6	1.94	2.06	0.58	9999
Kernouve	H6	1.78	1.92	0.56	8254
Kyushu	L6	1.94	2.07	0.61	8680
Middlesbrough	L6	1.90	2.02	0.58	6340
MIL99301	LL6	1.91	2.03	0.57	2921
Moorleah	L6	1.93	2.06	0.59	2653
Saratov	L4	2.00	2.12	0.62	2361
Tennasilm	L4	1.93	2.09	0.63	4014
Utrecht	L6	1.90	2.02	0.56	2445
Mean (<i>n</i> = 10)		1.91	2.04	0.05	

n = number of analyzed grains.

several dozens of ordinary chondrite falls (detailed results not shown here). The measured variations are almost within detection limit (Table 4) and exclude a significant contribution of superparamagnetic FeNi grains to the magnetic susceptibility of ordinary chondrites. Regarding the shape of the grains, using a mean susceptibility $K = (N + 1/3)/N(1 - N)$ for an ellipsoid of revolution where *N* is the demagnetization factor that depends on the aspect ratio of the ellipsoid, the misfit between the measured and theoretical M_S/χ for H and L chondrites requires *N* values of 0.08 or 0.75, indicating ellipsoid aspect ratio of 3 to 4 for prolate grains, and about 0.2 for oblate grains (e.g., Carmichael 1989). Furthermore, our XR microtomography found that all samples have a remarkably similar distribution of grain shape, with aspect ratio (ratio of maximum over minimum dimension) clustered around a mean value of 2.0 (Table 5). In all studied meteorites, about 50% of the grains are classified as equant, 30% prolate, 15% oblate, and 7% triaxial using Zingg criteria (Zingg 1935). Such a shape results in an approximately 18% increase in magnetic susceptibility with respect to spherical grains and is not enough to account for the observed discrepancy. Magnetic interactions are evidenced by the FORC properties (see First-Order Reversal Curve Properties section) and result in a higher magnetic susceptibility. Finally, metal grains with silicate or troilite inclusions, which are common in ordinary chondrites, have the same magnetic susceptibility as solid metal grains with the same shape, but lower M_S , again leading to a decrease in the M_S/χ ratio.

Because apparent magnetic susceptibility is increased by the combination of these effects, it cannot be used directly to estimate quantitatively the amount of metal in ordinary chondrites. M_S is a better proxy of the bulk metal content. However, the good correlation

between the two properties (Fig. 7) justifies the use of magnetic susceptibility for classification of ordinary chondrites (Rochette et al. 2003), all the more because susceptibility can be measured on much larger samples than hysteresis (up to several dozen grams), which allow averaging heterogeneities in composition.

Contribution of Kamacite and Tetrataenite

Combining the results from Mössbauer spectroscopy and chemical analyses (Table 1), the magnetic properties of the individual metallic phases (Table 2), and our measurements of meteorites, we obtain a picture of the contribution of each magnetic phase to the bulk magnetic properties of ordinary chondrites. Relative to the meteorite total mass, kamacite amounts to 16, 6.8, and 1.0 wt% in H, L, and LL chondrites, respectively (Table 1). This estimate was computed by combining the total abundance of metal determined by chemical analyses (Jarosewich 1990) and the kamacite fraction in the metal provided by Mössbauer for L and LL chondrites, and from chemical analysis for H chondrites (because only one H chondrite fall has been studied by Mössbauer spectroscopy [Danon et al. 1979b] and this measurement yielded an unrealistically high tetrataenite fraction of 18%). This translates into a contribution of kamacite of 89, 84, and 56% to the M_S of H, L, and LL chondrites, respectively. A reasonable estimate for M_{RS} of kamacite in ordinary chondrites can be derived from the hysteresis properties of H chondrites with the lowest coercivity that are dominated by multidomain kamacite and give $M_{RS}/M_S = 5 \times 10^{-3}$. This value is close to the value of 4×10^{-3} measured for a synthetic sample made of dispersed 10 μm pure iron grains by Bezaeva et al. (2010). Using a M_{RS}/M_S of 5×10^{-3} , we can estimate the contribution of kamacite to M_{RS} to 48, 22, and 3.0% in H, L, and LL chondrites, respectively. These numbers, which do not follow the trend for M_S , confirm the decoupling between induced and remanent properties in ordinary chondrites.

Hysteresis Properties, Metamorphism, Shock, and Irradiation

We have seen that the broad picture is the same for all ordinary chondrites, with induced magnetic properties (susceptibility and M_S) controlled by the amount of kamacite (except in some metal-poor LL chondrites), and the remanent properties increasingly influenced by tetrataenite from H to L to LL chondrites. However, it is noteworthy that in detail, different meteorites within the same class have significantly distinct hysteresis properties (Fig. 2). For

instance, coercivity of remanence varies from 9 to 453 mT in L chondrites, and from 5 to 335 mT in H chondrites. Therefore, hysteresis properties may reveal the different histories of these meteorites. Table 4 provides the average hysteresis properties as a function of class, petrographic type, and shock stage.

The scope of this study is not to discuss individual meteorites in detail, but rather to derive general mechanisms that can affect the magnetic properties. We identify three events that may affect the hysteresis properties of meteorites: thermal metamorphism, shock metamorphism, and irradiation. Thermal metamorphism affects the grain size of FeNi metal (Afiattalab and Wasson 1980; Easton 1983), modifies their mineralogy (e.g., Reisener and Goldstein 2003), and may anneal their defects. Shock metamorphism also affects the mineralogy (Taylor and Heymann 1971; Scorzelli et al. 1987; Ming et al. 1995; Bennett and McSween 1996; Smith and Goldstein 1997), the grain size (Friedrich et al. 2008) and the shape distribution (Gattacceca et al. 2005; Friedrich et al. 2008) of metal grains. Shock may also result in silicate darkening in which micron-sized metal blebs form in silicates (e.g., Bennett and McSween 1996; Van de Moortèle et al. 2007), and may lead to thermal annealing in some cases (Rubin 2004). Irradiation by protons has been shown to modify the magnetic properties of kamacite (Butler and Cox 1974), and irradiation by neutrons leads to ordering of taenite into tetrataenite (Paulevé et al. 1962). In natural settings, irradiation can occur at the surface of the parent body for regolith breccia samples, or while the meteorite is being transferred to the Earth under the form of a meter-sized meteoroid.

Because of the small size of the studied samples, it is not possible to provide a detailed discussion of the variation in the mass normalized magnetic properties like M_S , M_{RS} , or χ . These properties can be biased by nugget effects, especially in LL chondrites. However, it is noteworthy that in agreement with the strong decrease in magnetic susceptibility with increasing petrographic type observed in LL chondrites (Rochette et al. 2003), a similar trend is visible, although not as clearly, for M_S : $M_S = 6.3 \pm 2.3$ ($N = 8$) for LL3 and LL4, and $M_S = 3.6 \pm 1.9$ ($N = 17$) for LL5 and LL6 (Fig. 8a). This can be accounted for only in part by a higher proportion of tetrataenite versus kamacite and taenite in LL5 and LL6, and requires a higher bulk metal content in LL3 and LL4. Similarly, we observe a higher M_S , and hence a higher bulk metal content, in L3 and L4 ($M_S = 22.1$, $N = 7$) compared with L5 and L6 chondrites ($M_S = 16.6$, $N = 22$), and in H3 and H4 ($M_S = 44.8$, $N = 8$) compared with H5 and H6 chondrites ($M_S = 38.6$, $N = 16$). This is in agreement

with the decrease in the modal abundance of metal in ordinary chondrites as a result of oxidation during metamorphism (McSween and Labotka 1993).

Mass independent magnetic properties (e.g., B_C , B_{CR} , M_{RS}/M_S , and M_S/χ) can be interpreted with more confidence. B_{CR} and B_C increase with petrologic type in all classes (Fig. 8c, except for LL6 chondrites that are discussed below), which indicates that increasing thermal metamorphism is accompanied by increasing formation of tetrataenite. Among ordinary chondrites, this effect is most visible in LL chondrites that have the lowest amount of kamacite, which otherwise dilutes the tetrataenite signal. The increasing amount of tetrataenite with increasing metamorphism temperature is compatible with a lower cooling rate, allowing more diffusion of Ni in taenite during cooling above 400 °C, and eventually formation of tetrataenite by spinodal decomposition of this taenite below 400 °C. This overall inverse correlation between metamorphic grade and cooling rate would be compatible with an onion-shell model for the ordinary chondrite parent bodies (e.g., Kleine et al. 2009), at least while they cool in the subsolidus temperature range. However, recent metallographic cooling rate determination shows that this onion-shell model is likely not valid (Scott et al. 2013). A more plausible explanation is that metamorphism is accompanied by oxidation of metal in ordinary chondrites, as documented by the evolution with metamorphism of the iron content of silicates, of the relative abundances of silicates, and of the composition of metal (McSween and Labotka 1993; Rubin 2005; Dunn et al. 2010). The increasing Ni concentration in metal with increasing metamorphism as a result of oxidation will increase the tetrataenite abundance, as revealed by our measurements.

Notable exceptions are the LL6 chondrites that have significantly lower B_{CR} and M_{RS} than LL5 chondrites (Figs. 8b and 8c). This may be due to the formation of larger tetrataenite rims in these meteorites, because such rims have a multidomain behavior with lower B_{CR} than the smaller tetrataenite grains in the cloudy zone of taenite (Uehara et al. 2011). This process may not be visible in H6 and L6 chondrites because of the lower Ni content in the metal compared with LL. A good correlation between the width of the tetrataenite rim and the metallographic cooling rate has been found for IVA irons meteorites (Goldstein et al. 2009). Another explanation of the lower B_{CR} and M_{RS} in LL6 chondrites may be the increasing size of the tetrataenite particles in the cloudy zone. Again, tetrataenite grain size in the cloudy zone is correlated with the cooling rate at approximately 350–450 °C (Yang et al. 1997b). All together, this may indicate lower cooling rates in LL6 than in LL5 chondrites. M_S/χ variations are small

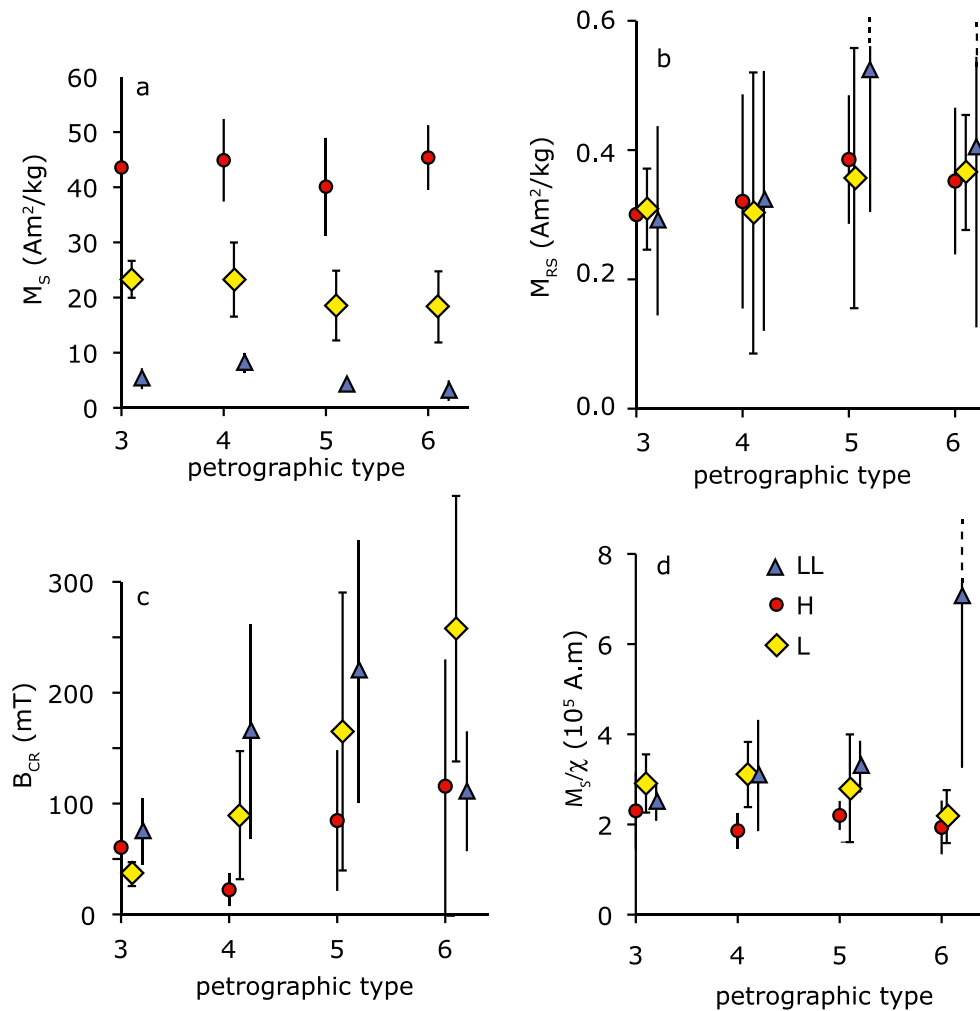


Fig. 8. Average hysteresis properties (± 1 SD) as a function of petrologic type for the three classes of ordinary chondrites. For L5 and L6 chondrites, our database purposely contains a large number of meteorites with shock stage $>S3$ (see Samples section). To avoid a bias, these heavily shocked meteorites are not included in the average values displayed here.

except for LL chondrites where this ratio increases with petrographic type, especially in LL6 chondrites (Fig. 8d). At the moment, we have no satisfactory explanation of this observation. Because remanent and induced properties are uncorrelated in ordinary chondrites, variations of B_{CR}/B_C and M_{RS}/M_S with thermal metamorphism, although significant, are also difficult to interpret.

In our database, only L chondrites display the full range of shock stages (S1–S6). The highly shocked L chondrites show significantly lower B_C , B_{CR} , M_{RS} , and M_{RS}/M_S compared with less shocked L chondrites (S1–S3). S4 meteorites have intermediate properties (Table 4, Fig. 9). This indicates a lower tetraenaite content in highly shocked L chondrites (S4–S6). This lower content can be explained in part by disordering by the shock wave, an effect that has been documented experimentally (Scorzelli et al. 1987). In particular, the

thermal excursion associated with the impact and the ensuing fast cooling result in disordering of the initial tetraenaite and decomposition into disordered Ni-rich ferromagnetic taenite (γ_2 phase). This is well in agreement with the postshock temperature increase above 600°C estimated for S5 and S6 shock stages (Stöffler et al. 1991). In view of the typical equilibrium temperatures of approximately 165 K encountered in the asteroid belt (e.g., Spencer et al. 1989), such temperature increases lead to postshock temperature above approximately 500°C , which is enough to disorder tetraenaite in a matter of minutes, although the knowledge of the disordering kinetics of tetraenaite as a function of temperature is still fragmentary (Wasilewski 1988). In S4 chondrites, it is likely that localized temperature excursions, as indicated by the presence of melt pockets and melt veins, result in localized disordering of tetraenaite. The effect of shock

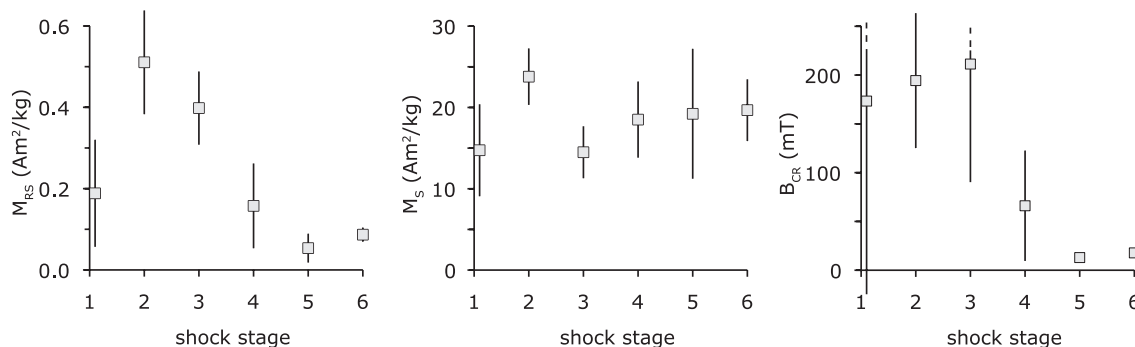


Fig. 9. Average hysteresis properties (± 1 SD) as a function of shock stage for L chondrites.

heating on the metallography has long been recognized (Taylor and Heymann 1971), in particular with the disappearance of cloudy taenite upon heating above approximately 500 °C (Scott 1973), the decomposition of martensite into plesite upon heating above 500 °C (e.g., Reisener and Goldstein 2003), and the formation of new martensite during rapid cooling from above approximately 700 °C (e.g., Yang et al. 1997a). But the magnetic signature of this transient heating event has never been documented.

Finally, we observe no correlation between the magnetic properties of the studied meteorites and the cosmic ray exposure age (Graf and Marti 1994, 1995) for H and LL chondrites. Irradiation does not produce a detectable influence on the magnetic properties of ordinary chondrites.

These general trends do not explain the unusual results obtained for a limited number of outliers. These deserve individual discussions that are beyond the scope of this study. As an example, Ste. Marguerite and Forest Vale, both unshocked H4, have distinctly lower M_{RS}/M_S than other H chondrites. This can be related to the distinctly high metallographic cooling rates (>1000 °C/Myr) measured for these two meteorites and attributed to excavation by impact (Scott et al. 2010). The fast and unusual cooling of Forest Vale has also been inferred from the study of Cr spinel and chromite (Wlotzka 2005) and recently confirmed to be as high as 10^4 °C/Myr (Ganguly et al. 2013). This fast cooling resulted in a limited or null amount of tetrataenite in these meteorites. This exemplifies the potential for magnetic measurements to detect samples with unusual cooling history.

It must be emphasized, however, that the interpretation of hysteresis properties is not unique. For instance, low B_{CR} values in L chondrites are characteristic of both L3 (in which no tetrataenite formed) and heavily shocked equilibrated L chondrites (in which tetrataenite has been disordered into taenite). Moreover, some individual results remain enigmatic.

For instance, the equilibrated L chondrite Mount Tazerzait (L5, S1) and Pê (L6, S1) have magnetic properties at the two extremes of the range covered by equilibrated L chondrites with $B_{CR} = 16$ and 453 mT, respectively, a discrepancy that remains unexplained.

Correlation with Microscopic Observations

It has been shown recently that the remanence carrier with the highest M_{RS} in ordinary chondrites is the cloudy zone of zoned taenite grains (i.e., submicron tetrataenite grains embedded in a kamacite/martensite matrix) (Uehara et al. 2011). The M_{RS} of larger tetrataenite grains, as found in the tetrataenite rim of zoned taenite or in zoneless plesite, is much lower, and that of kamacite even lower.

IRM acquisition curves for bulk samples of LL chondrites show three distinct components with coercivity peaking at <10 mT, approximately 60 mT, and approximately 650 mT, and extending up to 1.2 T (Fig. 10a). This was already observed in separated chondrules from Bjurböle L/LL4 chondrite (Acton et al. 2007). The same is observable in L chondrites (Fig. 10b). In H chondrites, the high-coercivity peak is faint but still visible (Fig. 10c). It is noteworthy that the two high-coercivity peaks correspond closely to the coercivity of remanence observed at microscopic scale for large tetrataenite grains and fine-grained tetrataenite in the cloudy zone (Uehara et al. 2012). The low-coercivity peak can be attributed to multidomain kamacite. It is also noteworthy that highly shocked chondrites lack the two high-coercivity peaks (Fig. 10d), which indicates that the original tetrataenite has been disordered. The drastic changes in magnetic properties associated with reheating events are demonstrated by the disappearance of the two high-coercivity peaks upon heating to 600 °C in controlled fugacity atmosphere for 20 min (Fig. 10c). This is additional proof that tetrataenite, with different domain states, is responsible for the two high-coercivity peaks of the coercivity spectrum.

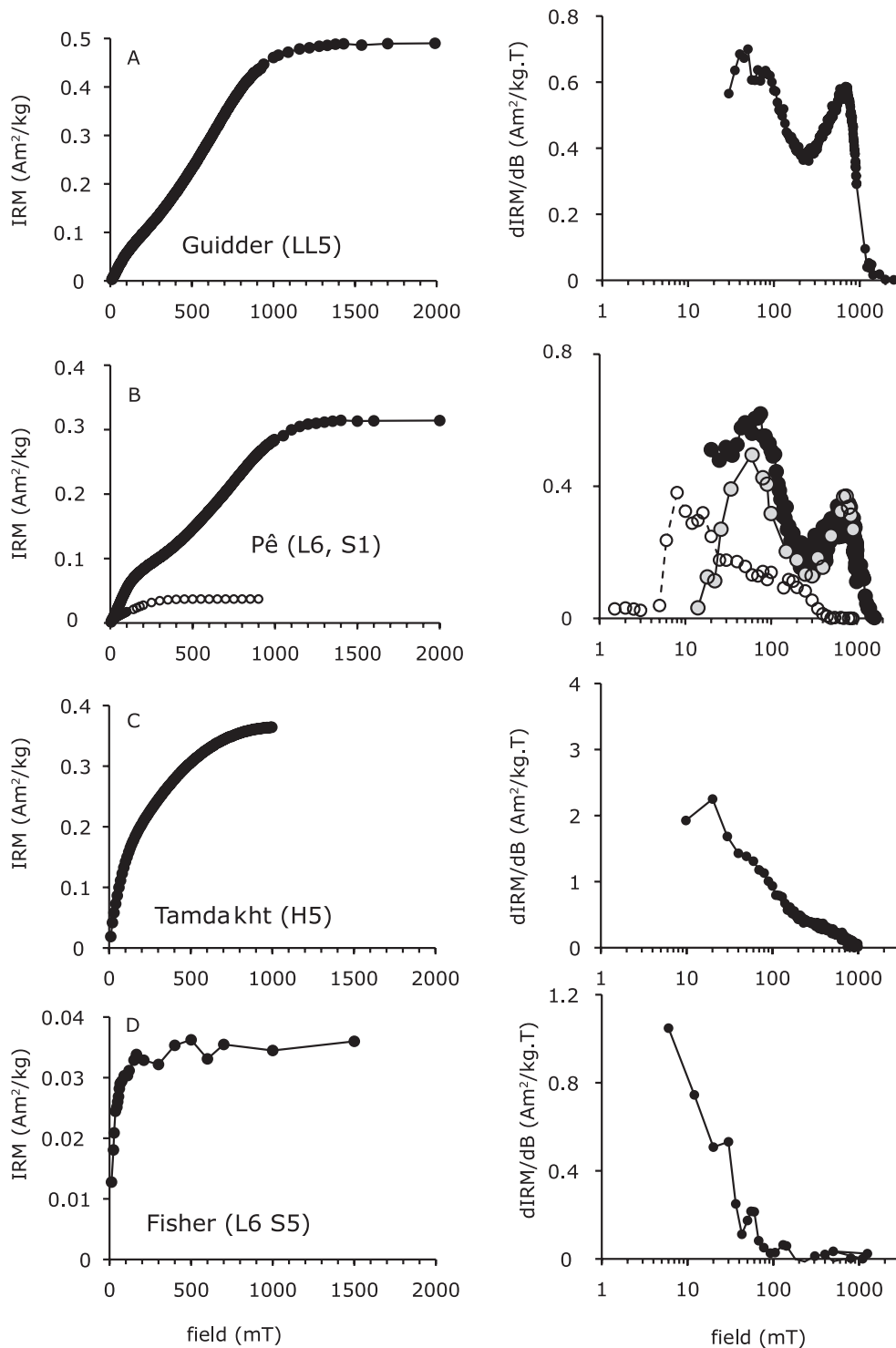


Fig. 10. IRM acquisition curves and their derivative for a selection of ordinary chondrites. For Pê (L6, S1), the gray circles (respectively, open circles and broken line) are the results after the sample was heated at 450 °C (respectively, 600 °C) for 20 min.

The size of tetraenaite grains in the cloudy zone of ordinary chondrites ranges from approximately 10 nm to approximately 100 nm (Yang et al. 1997a; Uehara

et al. 2011) and is related to the cooling rate of the meteorite in the 350–450 °C range (Yang et al. 1997b). This size range corresponds almost exactly to the size

range in which tetrataenite is in a single-domain magnetic state (7 nm to > 80–90 nm, see Introduction to Ferromagnetic Minerals in Ordinary Chondrites section). This single-domain behavior accounts for the high coercivity and high M_{RS} of the cloudy zone, as opposed to the low coercivity and low remanence of kamacite grains that are in multidomain state. The single-domain state of tetrataenite in the cloudy zone is also in good agreement with the high B_{CR} values (up to 1 T) measured at microscopic scale in this structure (Uehara et al. 2011) and with micromagnetic simulations (Bryson et al. 2014).

IMPLICATIONS FOR PALEOMAGNETISM

The understanding of the magnetic properties of the different FeNi minerals contained in ordinary chondrites has implications for their potential for paleomagnetic studies. In equilibrated ordinary chondrites, the possible carriers of a paleomagnetic record are kamacite, tetrataenite, and possibly ferromagnetic taenite. The situation is the same for the least primitive unequilibrated chondrites that have been heated above approximately 400 °C (allowing formation of tetrataenite), which correspond more or less to a petrologic type above 3.5 (Huss et al. 2006). Although kamacite has a simple behavior upon cooling, with no low-temperature martensitic transition, it is present in ordinary chondrites as large grains that have a strong multidomain behavior with typical $B_{CR}/B_C \sim 45$ and $M_{RS}/M_S \sim 0.005$, making them poor paleomagnetic recorders of dubious reliability (e.g., Tikoo et al. 2012). Tetrataenite can be found in a number of microstructures: in the cloudy zone of zoned taenite grains where it is found mostly as single-domain grains; in zoned plessite grains (in H and L equilibrated chondrites only, see Reisener and Goldstein 2003) as multidomain grains, or as massive multidomain grains in LL chondrites (Clarke and Scott 1980). Because of its high coercivity, single-domain tetrataenite in the cloudy zone may appear as an ideal paleomagnetic recorder. However, tetrataenite is a secondary mineral formed by ordering of a Ni-rich taenite precursor below the critical ordering temperature of 320 °C (Paulevé et al. 1962). Although it has been proposed that it may record the magnetization of its precursor taenite grain (e.g., Wasilewski 1988; Nagata and Funaki 1982), closer examination of the FeNi phase diagram shows that the precursor taenite grains become ferromagnetic only when cooling below 400 °C for the tetrataenite rim, and below 350 °C (maximum value) for the single-domain tetrataenite in the cloudy zone (Yang et al. 1997a; Uehara et al. 2011). As a consequence, the precursor taenite grains (with Ni

content approximately 50 wt% Ni and a Curie temperature of approximately 500 °C) can only record a magnetization when the temperature goes below 400 °C (for the rim) or below 350 °C (for the cloudy zone). This magnetization is either a thermochemical remanent magnetization or a partial thermoremanent magnetization acquired while cooling between 400 °C and 320 °C for the rim, and 350 °C and 320 °C for the cloudy zone.

It is not clear whether tetrataenite grains can inherit any remanent magnetization from their parent taenite grain. In any case, the single-domain tetrataenite in the cloudy zone can only record magnetic fields that are present after the meteorite has cooled below 350 °C (if it inherits the remanent magnetization of the precursor taenite) or 320 °C (if it does not). Therefore, slow cooling following thermal metamorphism down to 400 °C represents a time gap during which no paleomagnetic record can be preserved in equilibrated ordinary chondrites. The shortest time gap is obtained for type 4 chondrites (heated to about 700 °C; Huss et al. 2006) that have cooled relatively fast. For meteorites such as Bath, a H4 with a cooling rate of 80 °C Myr⁻¹ (Willis and Goldstein 1981), this time gap is only about 4 Myr. In view of the old age of the peak metamorphism temperature in ordinary chondrites, type 4 ordinary chondrites may well have cooled below 400–320 °C around 10 Ma after the formation of the solar system, but for type 6 chondrites, such cooling may require more than 100 Ma (Kleine et al. 2009; Henke et al. 2012).

For the most primitive ordinary chondrites (below petrographic type 3.5), the potential carriers of paleomagnetic information are kamacite and martensite. Magnetite and cohenite that have been reported in a few very primitive ordinary chondrites (Hutchison et al. 1987; Krot et al. 1997) are not discussed here. As in equilibrated chondrites, multidomain kamacite is a very poor paleomagnetic recorder, and martensite loses any potential paleomagnetic record of its precursor taenite when the martensitic transformation occurs (Momose et al. 1984) (although for most of the range of Ni-abundances over martensite forms, the parent taenite will have a Curie point below room temperature). Only single-domain kamacite present in dusty olivine grains appears to be a potential source of paleomagnetic information in unequilibrated ordinary chondrites (Uehara and Nakamura 2006; Lappe et al. 2011), although accessible only through magnetic microscopy.

CONCLUSION

We have shown that hysteresis properties measured on samples of a few tens of mg are distinctive intrinsic properties of individual ordinary chondrites, and we

provide a large data set of hysteresis properties of ordinary chondrite falls. The metal contents derived from magnetic measurements are in agreement with those estimated previously from chemical analyses. We evidence a decreasing bulk metal content with increasing petrologic type in ordinary chondrites, in agreement with progressive oxidation of metal with increasing thermal metamorphism. The bulk magnetic properties of ordinary chondrites can be approximated with a mixture of multidomain kamacite and tetrataenite. Kamacite dominates the induced magnetic properties in all ordinary chondrites, and two distinct populations of tetrataenite grains dominate the remanence properties. This picture derived from bulk magnetic properties is in very good agreement with microscopic observations, with a dichotomy between tetrataenite grains in the magnetic single-domain size range (7 nm to at least 80–90 nm) that are found in the cloudy zone of taenite grains, and larger ($> \mu\text{m}$) multidomain tetrataenite grains are found in plessite or in the rim of zoned taenite grains.

The presence of tetrataenite requires initial thermal metamorphism above 400 °C followed by slow cooling, with cooling rate of a few thousands °C Myr⁻¹ or lower in the subsolidus temperature range, which explains its absence in fast-cooled FeNi-bearing achondrites (e.g., HED and lunar meteorites) in which multidomain kamacite controls both the induced and the remanent magnetic properties. The bulk amount of tetrataenite is inversely correlated with the cooling rate above 400 °C (slower cooling allowing more diffusion of Ni), and the size of the tetrataenite precipitates in the cloudy zone and the thickness of tetrataenite rims are inversely correlated with the cooling rate. Therefore, the presence of tetrataenite, its distribution between different microstructures, and its grain-size distribution are controlled by the thermal history of the meteorites.

Highly equilibrated chondrites (types 5 and 6) have a higher tetrataenite content than type 4 chondrites. This may suggest lower cooling rates in the 650–450 °C interval, which would be supportive of an onion-shell model at least while cooling through this temperature interval, but a more likely origin for this observation is the increasing Ni content in metal with increasing metamorphism as a result of oxidation. In equilibrated chondrites, shock-related transient heating events above approximately 500 °C result in the disordering of tetrataenite into Ni-rich taenite, and an associated drastic change in magnetic properties (decrease in saturation remanence, coercivity, and coercivity of remanence). This effect is maximal for chondrites with shock stage S5 and S6, but is already visible starting from shock stage S4. As a good indicator of the amount of tetrataenite, hysteresis properties (in

particular, B_{CR} , M_{RS} , and the coercivity spectrum derived from IRM acquisition) are very sensitive proxies of the thermal history of ordinary chondrites. Both low cooling rates (during thermal metamorphism) and high cooling rates (following shock or thermal metamorphism) can be identified. Our data set strengthens the view that because of the poor paleomagnetic behavior of multidomain kamacite and the secondary nature of tetrataenite, equilibrated ordinary chondrites are challenging targets for paleomagnetic study.

Acknowledgments—The research leading to these results has received funding from Agence Nationale de la Recherche (project ANR-09-BLAN-0042), and People Programme (Marie Curie Actions) of the European Union's Seventh Framework Programme (FP7/2007-2013) under REA grant agreement N°298355. C.S. was supported by the European Commission through the Marie Curie Actions—RTNs ORIGINS (Project ID: 35519). C.S. and B.P.W. thank the Brown-Massachusetts Institute of Technology (MIT) NASA Lunar Science Institute, the NASA Origins Program, and Thomas F. Peterson, Jr. We thank the Muséum d'Histoire Naturelle de Paris for the loan of meteorites. Philippe Thomas (Meteoritica) kindly provided Chergach and Tamdakht samples. Rainer Bartoschewitz kindly provided Braunschweig samples. We acknowledge François Demory (CEREGE) for his help in the laboratory. This study benefited from constructive insights provided by J. I. Goldstein, G. Kletetschka, and associate editor E. R. D. Scott.

Editorial Handling—Dr. Edward Scott

REFERENCES

- Acton G., Yin Q.-Z., Verosub K. L., Jovane L., Roth A., Jacobsen B., and Ebel D. S. 2007. Micromagnetic coercivity distributions and interactions in chondrules with implications for paleointensities of the early solar system. *Journal of Geophysical Research* 112:B03S90.
- Afiattalab F. and Wasson J. T. 1980. Composition of the metal phases in ordinary chondrites: Implications regarding classification and metamorphism. *Geochimica et Cosmochimica Acta* 44:431–446.
- Arkani-Hamed J. 2005. Magnetic crust of Mars. *Journal of Geophysical Research* 100:E08005. doi:10.1029/2004JE002397
- Bennett M. E. and McSween H. Y. 1996. Shock features in iron-nickel metal and troilite of L-group ordinary chondrites. *Earth and Planetary Science Letters* 31:255–264.
- Bezaeva N. S., Gattacceca J., Rochette P., Sadykov R. A., and Trukhin I. 2010. Demagnetization of terrestrial and extraterrestrial rocks under hydrostatic pressure up to 1.2 GPa. *Physics of the Earth and Planetary Interiors* 179:7–20.

- Bland P. A., Zolensky M. E., Benedix G. K., and Sephton M. A. 2006. Weathering of chondritic meteorites. In *Meteorites and the early solar system II*, edited by Lauretta D. S. and McSween H. Y. Jr. Tucson, Arizona: The University of Arizona Press. pp. 853–867.
- Bryson J., Church N. S., Kasama T., and Harrison R. J. 2014. Nanomagnetic intergrowths in Fe-Ni meteoritic metal: The potential for time-resolved records of planetesimal dynamo fields. *Earth and Planetary Science Letters* 388:237–248.
- Butler R. F. and Banerjee S. K. 1975. Single-domain grain size limits for metallic iron. *Journal of Geophysical Research* 80:252–259.
- Butler R. F. and Cox A. V. 1974. The effect of neutron irradiation on remanent magnetization in multidomain iron and kamacite. *Journal of Geomagnetism and Geoelectricity* 26:55–71.
- Carmichael R. S. 1989. *Practical handbook of physical properties of rocks and minerals*. Boca Raton, Florida: CRC Press. 741 p.
- Clarke R. S. and Scott E. R. D. 1980. Tetrataenite—Ordered FeNi, a new mineral in meteorites. *American Mineralogist* 65:624–630.
- Collinson D. W. 1983. *Methods in rock magnetism and palaeomagnetism. Techniques and instrumentation*. London: Chapman and Hall. 503 p.
- Crangle J. and Hallam G. C. 1963. The magnetization of face-centred cubic and body-centred cubic iron + nickel alloys reviewed. *Proceedings of the Royal Society of London. Series A, Mathematical and Physical Sciences* 272:119–132.
- Danon J., Scorzelli R., Souza Azevedo I., Albertsen J. F., and Knudsen J. M. 1979a. Iron-nickel 50-50 superstructure in the Santa Catharina meteorite. *Nature* 277:283–284.
- Danon J., Scorzelli R., and Souza Azevedo I. 1979b. Iron-nickel superstructure in metal particles of chondrites. *Nature* 281:469–471.
- Dunlop D. J. and Kletetschka G. 2001. Multidomain hematite: A source of planetary magnetic anomalies? *Geophysical Research Letters* 28:3345–3348.
- Dunlop D. and Özdemir O. 1997. *Rock magnetism: Fundamentals and frontiers*. Cambridge, UK: Cambridge University Press. 573 pp.
- Dunn T. L., McSween H. Y. Jr., McCoy T. J., and Cressey G. 2010. Analysis of ordinary chondrites using powder X-ray diffraction: 2. Applications to ordinary chondrite parent-body processes. *Meteoritics & Planetary Science* 45:135–156.
- Easton A. J. 1983. Grain-size distribution and morphology of metal in E-chondrites. *Meteoritics & Planetary Science* 18:19–27.
- Egli R., Chen A., Winklhofer M., Kodama K. P., and Horng C.-S. 2010. Detection of non-interacting single domain particles using first-order reversal curve (FORC) diagrams. *Geochemistry Geophysics Geosystems* 11:Q01Z11, doi:10.1029/2009GC002916.
- Fabian K. 2006. Approach to saturation analysis of hysteresis measurements in rock magnetism and evidence for stress dominated magnetic anisotropy in young mid-ocean ridge basalt. *Physics of the Earth and Planetary Interiors* 154:299–307.
- Folco L., Rochette P., Gattacceca J., and Perchiazzi N. 2006. In situ identification, pairing and classification of meteorites from Antarctica through magnetic susceptibility measurements. *Meteoritics & Planetary Science* 41:343–353.
- Friedrich J. M., Wignarajah D. P., Chaudhary S., Rivers M., Nehru C. E., and Ebel D. S. 2008. Three-dimensional petrography of metal phases in equilibrated L chondrites—Effects of shock loading and dynamic compaction. *Earth and Planetary Science Letters* 275:172–180.
- Friedrich J. M., Ruzicka A., Rivers M. L., Ebel D. S., Thostenson J. O., and Rudolph R. A. 2013. Metal veins in the Kernouvé (H6 S1) chondrite: Evidence for pre- or syn-metamorphic shear deformation. *Geochimica et Cosmochimica Acta*. doi:10.1016/j.gca.2013.01.009.
- Funaki M., Nagata T., and Danon J. A. 1986. Magnetic properties of lamellar tetrataenite in Toluca iron meteorite. *Memoirs of National Institute of Polar Research, Special Issue* 41:382–393.
- Ganguly J., Tirone M., Chakraborty S., and Domanik K. 2013. H-chondrite parent asteroid: A multistage cooling, fragmentation and re-accretion history constrained by thermometric studies, diffusion kinetic modeling and geochronological data. *Geochimica et Cosmochimica Acta* 105:206–220.
- Gattacceca J., Rochette P., and Denise M. 2003. Magnetic properties of a freshly fallen LL ordinary chondrite: The Bensaour meteorite. *Physics of the Earth and Planetary Interiors* 140:343–358.
- Gattacceca J., Rochette P., Denise M., Consolmagno G., and Folco L. 2005. An impact origin for the foliation of ordinary chondrites. *Earth and Planetary Science Letters* 234:351–368.
- Gattacceca J., Rochette P., Gounelle M., and van Ginneken M. 2008. Magnetic anisotropy of HED and Martian meteorites and implications for the crust of Vesta and Mars. *Earth and Planetary Science Letters* 270:280–289.
- Goldstein J. I. and Michael J. R. 2006. The formation of plesite in meteoritic metal. *Meteoritics & Planetary Science Letters* 41:553–570.
- Goldstein J. I., Yang J., Kotula P. G., Michael J. R., and Scott E. R. D. 2009. Thermal history of IVA iron meteorites from transmission electron microscopy of the cloudy zone microstructure. *Meteoritics & Planetary Science* 44:343–358.
- Graf T. and Marti K. 1994. Collisional history in LL-chondrites. *Meteoritics* 29:643–648.
- Graf T. and Marti K. 1995. Collisional history of H chondrites. *Journal of Geophysical Research* 100:21247–21263.
- Henke S., Gail H.-P., Trieloff M., Schwarz W. H., and Thorsten K. 2012. Thermal history modeling of the H chondrite parent body. *Astronomy & Astrophysics* 545: A135.
- Hennemann O. D. and Siegel E. 1976. Spin-wave measurements of exchange constant A in Ni-Fe alloy thin films. *Physica Status Solidi (B)* 77:229–232.
- Herndon J. M., Rowe M. W., Larson E. E., and Watson D. E. 1976. Thermomagnetic analysis of meteorites, 3. C3 and C4 chondrites. *Earth and Planetary Science Letters* 29:283–290.
- Hopfe W. D. and Goldstein J. I. 2001. The metallographic cooling rate method revised: Application to iron meteorites and mesosiderites. *Meteoritics & Planetary Science* 36:135–154.
- Huss G. R., Rubin A. E., and Grossman J. N. 2006. Thermal metamorphism in chondrites. In *Meteorites and the early solar system II*, edited by Lauretta D. S. and McSween H. Y. Tucson, Arizona: The University of Arizona Press. pp. 567–586.

- Hutchison R., Alexander C. M. O'D., and Barber D. J. 1987. The Semarkona meteorite: First recorded occurrence of smectite in an ordinary chondrite, and its implications. *Geochimica et Cosmochimica Acta* 51:1875–1882.
- Jarosewich E. 1990. Chemical analysis of meteorites: Compilation of stony and iron meteorite analyses. *Meteoritics* 25:323–337.
- Kallemeyn G. W., Rubin A. E., Wang D., and Wasson J. T. 1989. Ordinary chondrites: Bulk compositions, classification, lithophile-element fractionations, and composition-petrographic type relationships. *Geochimica et Cosmochimica Acta* 53:2747–2767.
- Kleine T., Touboul M., Bourdon B., Nimmo F., Mezger K., Palme H., Jacobsen S. B., Yin Q.-Z., and Halliday A. 2009. Hf-W chronology of the accretion and early evolution of asteroids and terrestrial planets. *Geochimica et Cosmochimica Acta* 73:5150–5188.
- Kohout T., Kletetschka G., Kobr M., Pruner P., and Wasilewski P. J. 2004. The influence of terrestrial processes on meteorite magnetic records. *Physics and Chemistry of the Earth, Parts A/B/C* 29:885–897.
- Kohout T., Kletetschka G., Elbra T., Adachi T., Mikula V., Pesonen L. J., Schnabl P., and Slechta S. 2008. Physical properties of meteorites—Applications in space missions to asteroids. *Meteoritics & Planetary Science* 43:1009–1020.
- Kohout T., Jenniskens P., Shaddad M., and Haloda J. 2010. Inhomogeneity of asteroid 2008 TC₃ (Almahata Sitta meteorites) revealed through magnetic susceptibility measurements. *Meteoritics & Planetary Science* 45:1778–1788.
- Kong P. and Ebihara M. 1996. Metal phases of L chondrites: Their formation and evolution in the nebula and in the parent body. *Geochimica et Cosmochimica Acta* 14:2667–2680.
- Krol E. and Lang B. 1996. Magnetic properties of the recently fallen Baszkówka chondrite. Proceedings, 27th Lunar and Planetary Science Conference. p. 709.
- Krot A. N., Zolensky M. E., Wasson J. T., Scott E. R. D., Keil K., and Ohsumi K. 1997. Carbide-magnetite assemblages in type-3 ordinary chondrites. *Geochimica et Cosmochimica Acta* 61:219–237.
- Lappe S.-C., Church N., Kasama T., Bastos da Silva Fanta A., Bromiley G., Dunin-Borkowski R. E., Feinberg J., Russell S., and Harrison R. J. 2011. Mineral magnetism of dusty olivine: A credible recorder of pre-accretionary remanence. *Geochemistry Geophysics Geosystems* 12: Q12Z35, doi:10.1029/2011GC003811.
- Leroux H., Doukhan J.-C., and Perron C. 2000. Microstructures of metal grains in ordinary chondrites: Implications for their thermal history. *Meteoritics & Planetary Science* 35:569–580.
- Lovering J. F. and Parry L. G. 1962. Thermomagnetic analysis of co-existing nickel-iron metal phases in iron meteorites and the thermal histories of the meteorites. *Geochimica et Cosmochimica Acta* 26:361–382.
- Mayne R. G., McSween H. Y. Jr., McCoy T. J., and Gale A. 2009. Petrology of the unbrecciated eucrites. *Geochimica et Cosmochimica Acta* 73:794–819.
- McSween H. Y. and Labotka T. C. 1993. Oxidation during metamorphism of the ordinary chondrites of the ordinary chondrites. *Geochimica et Cosmochimica Acta* 57:1105–1114.
- Ming C., Xiande X., and El Goresy A. 1995. Nonequilibrium solidification and microstructures of metal phases in the shock-induced melt of the Yanzhuan (H6) chondrite. *Meteoritics* 30:28–32.
- Mishin Y., Mehl M. J., and Papaconstantopoulos D. A. 2005. Phase stability in the Fe-Ni system: Investigations by first-principles calculations and atomistic simulations. *Acta Materialia* 53:4029–4041.
- Momose K. and Nagai H. 1983. The application of thermomagnetic properties of Fe-Ni alloys to the thermal history of the Y-74646 chondrite. *Memoirs of the National Institute of Polar Research, Special Issue* 30:447–451.
- Momose K., Nagai H., and Muraoka Y. 1984. The martensitic transformation and the change of thermoremanent magnetization (TRM). *Memoirs of the National Institute of Polar Research, Special Issue* 35:298–301.
- Nagata T. 1988. Magnetic analyses of Antarctic chondrites on the basis of a magnetic binary system model. *Proceedings of the National Institute for Polar Research, Symposium on Antarctic Meteorites* 1:247–260.
- Nagata T. and Funaki M. 1982. Magnetic properties of tetrataenite-rich stony meteorites. *Proceedings of the Seventh Symposium on Antarctic Meteorites. Memoirs National Institute for Polar Research* 25:222–250.
- Nagata T. and Sugiura N. 1976. Magnetic characteristics of some Yamato meteorite—Magnetic classification of stone meteorites. *Memoirs of the National Institute of Polar Research Series C* 10:30–58.
- Nagata T., Sugiura N., and Schwerer F. C. 1975. Notes on magnetic properties of Yamato meteorites. *Memoirs of National Institute of Polar Research, Special Issue* 5:91–110.
- Nagata T., Funaki M., and Danon J. A. 1986. Magnetic properties of tetrataenite-rich meteorites II. *Memoirs of the National Institute of Polar Research, Special Issue* 41:364–381.
- Nagata T., Kaito C., Saito Y., and Funaki M. 1991. Tetrataenite in chondrites and experimental demonstration on formation of tetrataenite fine grains. *Proceedings of the National Institute for Polar Research, Symposium on Antarctic Meteorites* 4:404–419.
- Néel L., Pauthenet R., Laugier J., and Dautreppe D. 1964. Magnetic properties of an iron-nickel single crystal ordered by neutron bombardment. *Journal of Applied Physics* 35:873–876.
- Ozdemir O. and Dunlop D. J. 1997. Effect of crystal defects and internal stress on the domain structure and magnetic properties of magnetite. *Journal of Geophysical Research* 102:20211–20224.
- Paulevé J., Dautreppe D., Laugier J., and Néel L. 1962. Une nouvelle transition ordre-désordre dans FeNi (50-50). *Le Journal de Physique et le Radium* 23:841–843.
- Paulevé J., Chamberod A., Krebs K., and Bourret A. 1968. Magnetization curves of FeNi(50-50) single crystals ordered by neutron irradiation with an applied magnetic field. *Journal of Applied Physics* 39:989–990.
- Pesonen L. J., Terho M., and Kukkonen I. T. 1993. Physical properties of 368 meteorites: Implications for meteorite magnetism and planetary geophysics. *Proceedings of the National Institute for Polar Research, Symposium on Antarctic Meteorites* 6:401–416.
- Peters C. and Dekkers M. J. 2003. Selected room temperature magnetic parameters as a function of mineralogy, concentration and grain size. *Physics and Chemistry of the Earth* 28:659–667.

- Rambaldi E. R. and Wasson J. T. 1984. Metal and associated phases in Krymka and Chainpur: Nebular formational processes. *Geochimica et Cosmochimica Acta* 48:1885–1897.
- Rave W., Fabian K., and Hubert A. 1998. Magnetic states of small cubic particles with uniaxial anisotropy. *Journal of Magnetism and Magnetic Materials* 190:332–348.
- Reisener R. J. and Goldstein J. I. 1999. Microstructural and chemical study of Fe-Ni metal inside Semarkona chondrules (abstract #1868). 30th Lunar and Planetary Science Conference. CD-ROM.
- Reisener R. J. and Goldstein J. I. 2003. Ordinary chondrite metallography: Part 2. Formation of zoned and unzoned metal particles in relatively unshocked H, K, and LL chondrites. *Meteoritics & Planetary Science* 38:1679–1696.
- Reuter K. B., Williams D. B., and Goldstein J. I. 1989. Determination of the Fe-Ni phase diagram below 400 °C. *Metallurgical Transactions A* 20A:719–725.
- Rochette P., Sagnotti L., Bourot-Denise M., Consolmagno G., Folco L., Gattacceca J., Osete M. L. and Pesonen L. 2003. Magnetic classification of stony meteorites: 1. Ordinary chondrites. *Meteoritics & Planetary Science* 38:251–258.
- Rochette P., Gattacceca J., Chevrier V., and Lorand J.-P. 2005. Matching Martian crustal magnetization and meteorite magnetic properties. *Meteoritics & Planetary Science* 40:529–540.
- Rochette P., Gattacceca J., Bonal L., Bourot-Denise M., Chevrier V., Clerc J.-P., Consolmagno G., Folco L., Gounelle M., Kohout T., Pesonen L., Quirico E., Sagnotti L., and Skripnik A. 2008. Magnetic classification of stony meteorites: 2. Non-ordinary chondrites. *Meteoritics & Planetary Science* 43:959–980.
- Rochette P., Gattacceca J., Bourot-Denise M., Consolmagno G., Folco L., Kohout T., Pesonen L., and Sagnotti L. 2009. Magnetic classification of stony meteorites: 3. Achondrites. *Meteoritics & Planetary Science* 44:405–427.
- Rochette P., Gattacceca J., Ivanov A. V., Nazarov M. A., and Bezaeva N. S. 2010. Magnetic properties of lunar materials: Meteorites, Luna and Apollo return samples. *Earth and Planetary Science Letters* 292:383–391.
- Rubin A. E. 1994. Euhedral tetraenaite in the Jelica meteorite. *Mineralogical Magazine* 58:215–221.
- Rubin A. E. 2004. Postshock annealing and postannealing shock in equilibrated ordinary chondrites: Implications for the thermal and shock histories of chondritic asteroids. *Geochimica et Cosmochimica Acta* 68:673–689.
- Rubin A. E. 2005. Relationships among intrinsic properties of ordinary chondrites: Oxidation state, bulk chemistry, oxygen-isotopic composition, petrologic type, and chondrule size. *Geochimica et Cosmochimica Acta* 69:4907–4918.
- Sagnotti L., Rochette P., Jackson M., Vadeboin F., Dinares-Turrel J., Winkler A., and MAGNET Science team. 2003. Inter-laboratory calibration of low field and anhysteretic susceptibility measurements. *Physics of the Earth and Planetary Interiors* 138:25–38.
- Schultz L., Weber H. W., and Begemann F. 1990. Planetary noble gases in H3 and H4- chondrite falls. *Meteoritics* 25:405.
- Scorzelli R. B., Azevedo I. S., Danon J., and Meyers M. A. 1987. Mössbauer study of shock-induced effects in the ordered alloy Fe₅₀Ni₅₀ in meteorites. *Journal of Physics F: Metal Physics* 17:1993–1997.
- Scorzelli R. B., Azevedo I. S., and Funaki M. 1994. Tetraenaite in metallic grains of the Antarctic L6 chondrite ALHA76009. *Hyperfine Interactions* 91:535–539.
- Scott E. R. D. 1973. The nature of dark-etching rims in meteoritic taenite. *Geochimica et Cosmochimica Acta* 37:2283–2294.
- Scott E. R. D., Mandell D., Yang J., Goldstein J. I., Krot T., and Taylor G. J. 2010. Metamorphism and impacts on the parent asteroid of H chondrites (abstract #1529). 41st Lunar and Planetary Science Conference. CD-ROM.
- Scott E. R. D., Krot T., and Goldstein J. I. 2013. Thermal and impact histories of ordinary chondrites and their parent bodies: Constraints from metallic Fe-Ni in type 3 chondrites (abstract #1826). 44th Lunar and Planetary Science Conference. CD-ROM.
- Smith B. A. and Goldstein J. I. 1997. The metallic microstructures and thermal history of severely reheated chondrites. *Geochimica et Cosmochimica Acta* 41:1061–1072.
- Smith D. G. W., Miura Y., and Launspach S. 1993. Fe, Ni and Co variations in the metals of some antarctic chondrites. *Earth and Planetary Science Letters* 120:487–498.
- Sneyd D. S., McSween H. Y., Sugiura N., Strangway D. W., and Nord G. L. Jr. 1988. Origin of petrofabrics and magnetic anisotropy in ordinary chondrites. *Meteoritics* 23:139–149.
- Spencer R. S., Lebofsky L. A., and Sykes M. V. 1989. Systematic biases in radiometric diameter determinations. *Icarus* 78:337–354.
- Stöffler D., Keil K., and Scott E. R. D. 1991. Shock metamorphism of ordinary chondrites. *Geochimica et Cosmochimica Acta* 55:3845–3867.
- Sugiura N. 1977. Magnetic properties and remanent magnetization of stony meteorites. *Journal of Geomagnetism and Geoelectricity* 29:519–539.
- Taylor G. J. and Heymann D. 1971. The formation of clear taenite in ordinary chondrites. *Geochimica et Cosmochimica Acta* 35:175–188.
- Terho M., Pesonen L. J., and Kukkonen I. T. 1992. Petrophysical classification of meteorites: New results. Open File Report. Q 29.1/91/1, Geophys. Dep. Geol. Surv. Finl., 40 p.
- Tikoo S. M., Weiss B. P., Buz J., Lima E. A., Shea E. K., Melo G., and Grove T. L. 2012. Magnetic fidelity of lunar samples and implications for an ancient core dynamo. *Earth and Planetary Science Letters* 337–338:93–103.
- Uehara M. and Nakamura N. 2006. Experimental constraints on magnetic stability of chondrules and the paleomagnetic significance of dusty olivines. *Earth and Planetary Science Letters* 250:292–305.
- Uehara M., Gattacceca J., Leroux H., Jacob D., and Van der Beek C. J. 2011. Magnetic microstructures of metal grains in equilibrated ordinary chondrites and implications for paleomagnetism of meteorites. *Earth and Planetary Science Letters* 306:241–252.
- Uehara M., Gattacceca J., Rochette P., Demory F., and Valenzuela E. M. 2012. Magnetic study of meteorites recovered in the Atacama desert (Chile): Implications for meteorite paleomagnetism and the stability of hot desert surfaces. *Physics of the Earth and Planetary Interiors* 200–201:113–123.
- Van de Moortèle B., Reynard B., Rochette P., Jackson M., Beck P., Gillet P., McMillan P. F., and McCammon C. A. 2007. Shock-induced metallic nanoparticles in olivine-rich

- Martian meteorites. *Earth and Planetary Science Letters* 262:37–49.
- Van Schmus W. R. and Wood J. A. 1967. A chemical-petrologic classification for the chondritic meteorites. *Geochimica et Cosmochimica Acta* 31:747–765.
- Wasilewski P. 1981. Magnetization of small iron-nickel spheres. *Physics of the Earth and Planetary Interiors* 26:149–161.
- Wasilewski P. 1988. Magnetic characterization of the new magnetic mineral tetrataenite and its contrast with isochemical taenite. *Physics of the Earth and Planetary Interiors* 52:150–158.
- Wasilewski P., Acuña M. H., and Kletetschka G. 2002. 433 Eros: Problems with the meteorite magnetism record in attempting an asteroid match. *Meteoritics & Planetary Science* 37:937–950.
- Weiss B. P., Gattacceca J., Stanley S., Rochette P., and Christensen U. R. 2010. Paleomagnetic records of meteorites and early planetesimal differentiation. *Space Science Reviews* 152:341–390.
- Wieczorek M. A., Weiss B. P., and Stewart S. T. 2012. An impactor origin for lunar magnetic anomalies. *Science* 335:1212–1215.
- Willis J. and Goldstein J. I. 1981. A revision of metallographic cooling rate curves for chondrites. Proceedings, 12th Lunar and Planetary Science Conference. pp. 1135–1143.
- Wlotzka F. 2005. Cr spinel and chromite as petrogenetic indicators in ordinary chondrites: Equilibration temperatures of petrologic types 3.7 to 6. *Meteoritics & Planetary Science* 11:1673–1702.
- Yang C. W., Williams D. B., and Goldstein J. I. 1997a. Low-temperature phase decomposition in metal from iron, stony-iron, and stony meteorites. *Geochimica et Cosmochimica Acta* 61:2943–2956.
- Yang C. W., Williams D. B., and Goldstein J. I. 1997b. A new empirical cooling rate indicator for meteorites based on the size of the cloudy zone of the metallic phases. *Meteoritics & Planetary Science* 32:423–429.
- Zhang J., Williams D. B., Goldstein J. I., and Clarke R. S. 1990. Electron microscopy study of the iron meteorite Santa Catharina. *Meteoritics* 25:167–175.
- Zingg T. 1935. Beitrag zur Schotteranalyse. Ph.D. thesis, Eidgenössische Technische Hochschule, Zürich, Switzerland.
-